EUROPEAN ORGANIZATION FOR NUCLEAR RESEARCH

CERN–PPE/92-19

February 7, 1992

The Laser System for Calibration and Monitoring of the OPAL Jet Chamber

O. Biebel[1], B. Boden[1], H. Börner[2a], H. Breuker[2], S. Bug[1], A. Eyring[1], H.M. Fischer[1], C. Geich-Gimbel[1], S. Gross[1], J. Hagemann[2b], M. Hauschild[2], R.D. Heuer[2], K. Karner[2], G. Knop[1], S. Levegrün[1], G. Linser[2], G. Maringer[1], E. Mauer[1], U. Maur[1], B. Nellen[1], H. Neumann[1c], A. Rollnik[1], O. Runolfsson[2], H. von der Schmitt[3], S. Schreiber[1], W. Seidl[2], A. Simon[1], J. Thiebes[1], D. Voillat[2], A. Wagner[3b], P. Wicht[2], B. Wolf[1d], B. Wünsch[1e]

[1]Physikalisches Institut, Universität Bonn, D-5300 Bonn 1, Germany
[2]CERN, European Organization for Nuclear Research, CH-1211 Geneva 23, Switzerland
[3]Physikalisches Institut, Universität Heidelberg, D-6900 Heidelberg, Germany
[a]now at Philips Hamburg, D-2000 Hamburg, Germany
[b]now at DESY, D-2000 Hamburg 52, Germany
[c]now at Fatherboard Computer GmbH, D-5653 Leichlingen, Germany
[d]now at Universität Mainz, D-6500 Mainz, Germany
[e]now at Deutsche Telepost Consulting GmbH, D-5300 Bonn, Germany

Abstract

In this report we describe the construction and performance of the laser system which was used in Summer 1989 for the initial calibration of the OPAL jet chamber after installation on the LEP beam axis and which has served as a monitoring tool since then. Two Nd:YAG lasers are used to generate 48 high precision double beams which enter the chamber at fixed positions. The main features of the roughly 450 optical components are described and the beam alignment procedures are explained. Results are given for jet chamber calibration constants such as drift velocity, Lorentz angle, and residual sagittas.

(Submitted to Nuclear Instruments and Methods)

1 Introduction

The main part of the central tracking device of the OPAL experiment at the LEP e^+e^--collider at CERN consists of a pictorial jet chamber with diameter and length both of about 4 m. Details of the detector construction and first running experience were reported in [1],[2]. Since the scale and complexity of the chamber are very much increased with respect to earlier tracking detectors, new methods for calibration and monitoring had to be developed.

The concept of simulating particle tracks by use of ultraviolet (UV) laser beams has been shown to be very useful (see [3] for a review). In this article we describe the design and construction of a calibration system based on UV laser beams for the OPAL jet chamber.

The laser calibration of the jet chamber was performed in several steps. After initial tests with a full scale prototype [4], a laser scan of the entire detector volume was performed in the autumn of 1988. This was done with the help of a fully rotatable scan mirror located in the centre of the chamber at the nominal vertex position. After installation of the detector on the LEP beam axis in the spring of 1989 a new stationary system was used to calibrate the chamber, for the first time inside the magnetic field of 0.435 T. This system is able to give a fast survey over the different detector parameters to be monitored.

A well understood calibration makes it possible to perform online reconstruction of the jet chamber data including pattern recognition. This allows background events to be rejected at a second trigger level, important for the anticipated high event rate on the Z^0 peak. Another aspect is the monitoring and calibration during the low event rate expected at LEP running above the W^+W^- threshold. Here a continuous calibration using data from e^+e^--interactions is limited by statistics.

In this article we first give a brief description of the jet chamber in section 2. We then explain in section 3 the basic methods for chamber calibration by use of laser beams. In section 4 the details of the optical beam transport system are given. An overview on the alignment procedures applied follows in section 5. Section 6 describes the laser beam detection and the feedback system for the beam steering. Section 7 gives details of the performance and running experience, and concludes with the determination of calibration constants as obtained with the new laser system.

2 Jet Chamber

The OPAL jet chamber is of cylindrical shape, with an outer diameter of 3.7 m and an inner diameter of 0.5 m. It is subdivided into 24 identical sectors, each covering 15° in azimuth. Each sector contains one radial sense wire plane and is separated from the neighbouring sectors by two radial cathode wire planes. All wire planes are stretched between two conical end plates which are held apart by a shell of 24 aluminium panels at the outer chamber radius. The wire length increases from 3.2 m to 4.0 m going from inside to outside. Each sense wire plane consists of 159 sense wires separated by 10 mm, alternating with potential wires. The location of the sense wires extend from a radius of 255 mm at the inside to 1835 mm at the outside, thus resulting in maximum drift distances ranging from 3 to 25 cm. In order to resolve the left-right ambiguity the sense wires are mechanically staggered by $\pm 100\,\mu$m. The sense wires are grounded and the voltage applied to the potential wires for the adjustment of the gas gain is -2.38 kV. A homogeneous drift field is provided by applying voltages ranging from -2.5 kV at the inner to -25 kV at the outer cathode wires. The correct field termination is provided by field shaping electrodes on all boundaries of the sensitive chamber volume. The working

point was chosen to provide a drift field of 890 V/cm, where the drift velocity is approximately saturated at a value of 52.7 μm/ns. A three component gas mixture of 88.2% argon, 9.8% methane and 2.0% isobutane is used at a pressure of 4 bar.

The read out electronics is based on a 100 MHz flash analogue-to-digital converter (FADC) system [5] with 2 channels per sense wire. At each wire the three-dimensional coordinates of a particle track are determined from wire position, drift time, and a charge division measurement.

3 Principles of Jet Chamber Calibration by Use of Laser Beams

3.1 Ionization

Ionization in drift chamber gases by means of UV laser beams has already been observed by various groups [6]. The photon energy of UV lasers is in the range of only 3 to 5 eV. This is not sufficient to ionize usual drift chamber gases which have ionization thresholds from 11 to 16 eV. However, it has been shown that the UV light ionizes residual traces of hydrocarbons in chamber gases via 2-photon absorption processes [7].

The concentration of these hydrocarbons is usually kept as low as possible by means of gas cleaning systems. Purity of drift chamber gases is important to achieve optimal operating conditions and to avoid early ageing of the chamber. Nevertheless, the amount of these hydrocarbons seems to be stable, presumably due to the outgasing of chamber materials.

After continuous gas cleaning over several months the gas used at the full scale prototype of the jet chamber was analysed with gas-chromatographic methods. Several aromatic and aliphatic hydrocarbons such as phenol, benzene, toluene and xylene were detected with concentrations at the ppm level [8].

In the present calibration system two frequency quadrupled Nd:YAG lasers at a wavelength of 266 nm (4.68 eV) are used. Ionization is achieved with moderate energy densities. About 10 μJ/mm^2 are sufficient for an ionization level equivalent to a minimum ionizing particle. After two years of operation of the jet chamber at LEP, no decrease in the ionization produced by the laser was observed. The gas system of the jet chamber was built as a closed system with recirculation and purification of the gas [9]. The continuous gas cleaning did not affect the amount of ionizable substances in the jet chamber gas.

The ionization density is homogeneous along the laser beam track and fluctuations are small. Since laser tracks do not produce clusters or δ-rays the ionization obeys Poisson instead of Landau statistics. Since such tracks are, in addition, not affected by multiple scattering, good resolution in space and time is obtained.

3.2 Basic Calibration Constants

The coordinates of a particle traversing the jet chamber in the plane perpendicular to the sense wires, the r-ϕ plane[1], are determined by drift time measurements and the knowledge of the geometrical wire positions, the drift velocity and the Lorentz angle. The z coordinates along the sense wires are determined using resistive charge division.

The laser beam is considered to be perfectly straight. The residual measured sagitta of a laser track is of the order of a few μm, resulting in a negligible timing error of less than 0.1 ns. All

[1] Throughout this article the standard OPAL coordinate system is used. The origin is at the nominal interaction point. The x axis is horizontal and points approximately towards the centre of LEP. The y axis is approximately vertical and the z axis is in the e^- beam direction. The polar angle θ is measured from the z axis and the azimuthal angle ϕ from the x axis about the z axis.

measured deviations from a straight line are due to wire dependent time offsets, uncertainties in the knowledge of the geometrical wire positions or, to a lesser extent, inhomogeneities of the drift field.

Drift velocity and Lorentz angle are important calibration constants for drift chambers. For the jet chamber the drift velocity has to be continuously monitored to better than 0.1% in order to maintain its excellent spatial resolution of about 130 μm in r-ϕ. The laser system provides a direct method to measure the drift velocity with the required accuracy. In this system, two parallel laser beams with a spacing of 10 mm are used. Figure 1a shows a sector in the r-ϕ plane, illustrating the laser double beam inside the jet chamber. The drift velocity is obtained by measuring the difference in arrival time of the signals produced by this double beam.

In order to measure the momentum of charged particles, a homogeneous magnetic field of $B = 0.435$ T along the LEP beam direction is applied. The magnetic field leads to a rotation of the effective drift path of the electrons by the Lorentz angle α_L, which is about 20°. In combination with the measurement of drift velocity the Lorentz angle can be determined.

The charge deposited on the sense wire is divided according to the ratio of the resistances at the two wire ends. This ratio is a function of the position along the wire. Thus, the measurement of the charges at both sense wire ends allows the determination of the z coordinate. The gains at both wire ends may be different, due to possible small differences in amplification and pulse attenuation. The coordinate is normalized by an effective wire length, depending on the impedance of the wire and preamplifier. The effective wire lengths and gains are calibration constants. They can be determined from the knowledge of the laser beam positions in z. Figure 1b shows an overview of the jet chamber in the r-z plane, indicating the laser beams.

4 Description of the Laser Beam Path

An overview of the OPAL experimental area is given in figure 2 showing the components of the laser system. The calibration system provides two groups of 24 laser beams, one for each half-sector, arranged in complementary configurations on both sides of the detector. To obtain calibration constants only one beam at any given time is used.

The beams for each group are provided by a Nd:YAG laser situated in a cabin outside the detector. The laser beam is directed onto the main mirror. With the main mirror one out of 24 channels is selected. It reflects the laser beam towards the distributor wheel, from where it is reflected parallel to the LEP beam axis towards the detector. The lasers and main mirrors are accessible during standard LEP operation. After passing into the pressure vessel, each beam is again reflected three times at the mirror support cone before it hits the beamsplitter, from where it is injected into the chamber. The full track length from the laser to the outermost wire of the jet chamber varies from 14.3 m to 16.1 m, different for each sector.

In the following sections we first give a description of the laser and the optical components, followed by an explanation of the mirror system which is used to guide the laser beams from their origin towards the chamber. Finally, the positions of the laser beams inside the active volume of the jet chamber are described.

4.1 Laser and Optical Components

On both sides of the detector, the lasers and optical components are located in cabins at the height of the LEP beam pipe, 6 m above ground level.

The cabins, made of sheet metal, are hermetic in order to suppress electromagnetic noise generated by the laser flash lamps or the high voltage switching of the laser Pockels cells. The

optical benches which carry the lasers and optical components are mounted on heavy iron structures. These are fixed to the walls of the underground cavern in order to keep vibrations at a minimum.

The Nd:YAG lasers [10] are operated in a Q-switched mode to obtain high power laser pulses. The pulse length is of the order of 3 to 4 ns. The frequency is doubled 2 times by temperature stabilized doubler crystals yielding a wavelength of $\lambda = 266$ nm. To obtain a gaussian spatial beam profile together with a low divergence, the lasers are operated in the TEM_{00} mode. Calibration and monitoring is performed with an energy density of approximately 50 $\mu J/mm^2$. A higher ionization level than that produced by a minimum ionizing particle is used in order to achieve optimal resolution.

The optical components mounted on the optical bench are shown in figure 3. The laser beam first passes a thin quartz plate, followed by a Pockels cell, a half-wave plate, a mechanical beam shutter and a Galilean telescope.

The quartz plate (thickness 1 mm) has an antireflective coating on its backside and reflects 1% of the incoming light under 90° onto a fast vacuum photo diode [11]. The output signal of the diode is used to trigger the jet chamber readout system and the readout of the beam position monitors. It is also used to measure the laser beam energy.

The Pockels cell [12] switches the polarization plane by 90° for every second shot. This is used to obtain an alternating laser double beam as described in section 7.3. The half-wave plate [13] determines the absolute orientation of the polarization plane, which has to be different for each individual channel. This is required because of the different azimuthal orientations of the beamsplitters. To adjust the appropriate polarization, the half-wave plate is rotated using direct current motors. Its angle is measured by an angular encoder [14] with a resolution of 0.036°.

The Galilean telescope provides a soft focus of the beam with a long focal length of about 13 m, near anode wire 80 inside the chamber. It consists of a biconvex quartz lens of focal length 160 mm and a plano-concave quartz lens of focal length -46 mm. Since the lengths of the beam paths differ by up to 1.8 m from channel to channel, the telescope focus has to be varied. The distance between the lenses is measured with an encoder, resulting in a resolution of the focal length of 0.9 cm per count. The half-wave plate as well as the adjustment of the focal length are controlled by a microprocessor.

The beam width inside the jet chamber stays practically constant for all 159 wires. It is 0.8 mm (FWHM) with a beam divergence of less than 0.4 mrad. The beam width and divergence were measured in the laboratory with a high resolution (15 μm) linear photo diode array [15] at various distances around the focal point. The pulse length of 3 to 4 ns as well as the beam width are sufficiently small to avoid unacceptable broadening of the ionization signals.

The mirrors used in this system consist of glass substrate [16] with dielectric coatings. For beam detection, light is partially transmitted through some of the mirrors. These special mirrors are made of synthetic quartz [17]. The error on the surface planarity of all mirrors is better than 2 μm. Optimal reflectivity is obtained by optimising the dielectric coatings for the individual angles of reflection and the wavelength of the laser [18].

A tube system all along the laser beam path is necessary for safety reasons and also to avoid material accidentally blocking the beam. Outside the pressure vessel the tubes are made of aluminium with an inner diameter of 25 mm. All other protection tubes are made of plexi glass, 10 mm in diameter. The aluminium tubes have an inner layer of non reflective, absorptive material to avoid any laser beams entering the jet chamber by reflections. The beams are passed into the pressure vessel through quartz windows of 10 mm thickness.

4.2 Main Mirror

The main mirror has the central task to feed the laser beam into a preselected channel. A design principle is the possibility to allow beam position corrections necessary to deal with small misalignments, mechanical settlements or deformation under stress. Since the underground cavern is climatized changes due to temperature are not a problem.

The required positioning accuracy is determined by the maximal beam path length of about 10 m from the mirror to the jet chamber and the necessary reproducibility of the beam position on the beamsplitter. This was determined to be $\pm$ 0.5 mm, yielding to an acceptable error on angle of the order of 50 μrad.

The main mirror allows three dimensional beam steering. A straight laser track in space can be described by a set of four parameters in a unique way: two for its direction and two for its start point in its plane of origin. Therefore, the main mirror has two rotational (θ, ϕ) and two lateral (y, z) degrees of freedom.

It consists of three individual mirrors (M1, M2, M3) mounted on a platform which is supported by the radiation shielding of the experiment. The principal components are shown in figure 4. The stationary mirror M1 reflects the incoming laser beam along the y direction onto mirror M2, from where it is reflected along the z direction. Mirror M3 is rotatable around the y axis by the polar angle θ and around z direction by the azimuthal angle ϕ. It sits on a translation stage movable along the z direction. This stage together with mirror M2 are mounted on an additional stage which is movable along the y direction. This arrangement ensures the mutual independence of the four degrees of freedom or, in other words, decouples the movements in all four space coordinates.

All movements are induced by dc motors with suitable chosen transmissions [19]. The mirror positions are measured by incremental encoders whose values are read out by specially designed electronics which steers the motors under microprocessor control. The linear movements of the translation stages [20] are measured by linear rulers [14] leading to a position accuracy of 5 μm. The accessible range is 100 mm in y direction and 50 mm in z direction. The rotation tables for the angular movements of M3 are equipped with precision bearings [21]. The angular positions of M3 are measured by angular encoders [14] which are connected directly to the rotation axis. The resolution in angle is 17.45 μrad, leading to an accuracy in the laser beam angle of 34.9 μrad in θ and 17.45 μrad in ϕ.

4.3 Distributor Wheel

The two distributor wheels (see figure 5a) are mounted onto the iron forward radiation shielding which is part of the OPAL magnet, thus minimizing any possible vibrations. The support structure for mirrors and beam detectors is made of aluminium. The 24 mirrors per side (M4) reflect the laser beam into the z direction. They are mounted at a radius of 467 mm. All of them are equipped with two micrometers [22] for polar and azimuthal positioning of the mirrors (figure 5b). A 1 mm quartz plate sitting directly behind the mirror reflects about 5% of the beam onto a beam detector. Mirror M4 is transparent thus allowing visual inspection of the beam path between distributor wheel and the jet chamber pressure vessel. Additional outer mirrors (M4') are necessary for those channels which are on the away side of the laser in order to bypass the LEP mini β quadrupole. Two Helium-Neon lasers are mounted on each distributor wheel. These are aligned in such a way that their beams overlap in the centre of mirror M3. Their purpose is to give a fast indication of the relative position of the distributor wheel with respect to the main mirror. The distributors are supported on brass bearings which allow three

dimensional alignment of the structures as a whole.

4.4 Mirror Support Cone

Inside the pressure vessel the laser beam is reflected three times before it enters the jet chamber. This is necessary in order to leave a 120 mrad cone free of material in front of the forward luminosity detector. The support structure for the mirrors M5, M6, and M7, the mirror support cone, is shown in figure 6. The design criteria for the cones, which are identical for both sides, were a) to use a minimum of magnetizable material, b) to achieve high rigidity, and c) to use the restricted space not occupied by jet and vertex chamber electronics and cables. The support cones are made of fibre epoxy mounted on aluminium rings. The whole structure is fixed onto the end flanges of the jet chamber. All mirror mounts are machined out of aluminium and were adjusted by the use of small setscrews. Since the beam paths on the support cone are short compared to the outer beam sections, micrometers were not necessary in this case.

After passing through a scintillating monitor, the incoming laser beam is reflected by 90° at mirror M5 towards the LEP beam pipe. The scintillating monitors have a central hole with a diameter of 12 mm. About 5% of the laser beam passes through mirror M5 onto a planar photo diode to measure its position. The laser beam is reflected at mirror M6 by 97° and at mirror M7 by 90°. Finally it passes through the beamsplitter into the jet chamber. For 12 out of the 48 channels the position of the laser beam is measured a third time behind M7 using non-magnetic planar photo diodes. The beamsplitters divide the laser beams into two parallel beams with a spacing of 10 mm. They are passed through holes of 18 mm diameter into the jet chamber. In order to allow for a large enough gap for the laser beams, four inner field wires were omitted for each half-sector at the inner radius of the chamber.

The beamsplitters together with the last mirror M7 are mounted in special holders, as shown in figure 6c. To avoid any mechanical pressure on the beamsplitters, they are held by springs. This is important, because any deformation of the beamsplitters leads to a deviation of the double beam parallelism, depending on the point of incidence.

The beamsplitters are made of high quality quartz [17] and manufactured with the appropriate high precision. The nominal thickness of the quartz substrate is 13.1 mm and the angle of incidence was chosen to be 49.2°. Special coatings provide the beam splitting with negligible losses due to absorption, reflection or refraction [18]. The individual coatings are : antireflective for in- and outgoing beams, a 100 % mirror layer, and a polarization dependent beam splitting coating. The latter is designed in a way such that energy sharing between the two beams depends on the incident laser beam polarization and is therefore adjustable in a wide range. The design double beam distance is $\Delta s = 10,007.5\,\mu$m $\pm 0.4\%$ (refractive index n = 1.5), the parallelism is better than 75 μrad.

However, the double beam distance and the parallelism have to be known with an accuracy of better than 0.1% to achieve the appropriate precision on the measurement of the drift velocity. This made it necessary to measure them individually for each of the 48 beamsplitters. A high resolution CCD camera [23] with a pixel width of 23 μm was used to determine the double beam distance at various distances from the beamsplitter. To guarantee the nominal incident angle of the laser beam, these measurements were done with the splitters and mirrors M7 already mounted in their holders. From these measurements the distance is known with a precision of better than 4 μm, the deviation from the parallelism better than 1 μrad. The measured beam distance is corrected for the different refractive index of the jet chamber gas mixture.

4.5 Laser Beam Position inside the Active Jet Chamber Volume

An overview of the azimuthal and polar orientations of the laser beams inside the jet chamber is shown in figure 1a and b, respectively.

For each of the 48 half-sectors a laser double beam can be provided. In ϕ, their location is at the centre of each half-sector. They originate from positive z coordinates (z = 1200, 1250 mm) for the right hand half-sectors ($-\phi$) and from negative z coordinates (z = -1200, -1250 mm) for the left hand half-sectors ($+\phi$). The radius with respect to the LEP beam axis is 234 mm. The beams are staggered by 50 mm in z direction to achieve higher rigidity for the vertex chamber support tubes. These are two aluminium cylinders with a thickness of 2 mm which hold the vertex chamber inside the jet chamber; 48 holes were drilled into these tubes in order to feed through the laser beams. This staggering also gains space for cables, pipes and other material necessary to operate the vertex chamber. All beams are inclined by 7° with respect to the vertical plane. The laser beams thus provide decreasing z coordinates with increasing radial distance. The laser beams are finally absorbed at the outer field shaping electrodes. The absolute azimuthal angles ϕ and polar angles θ of the laser beams are known within 2.2 mrad and 1.4 mrad respectively. This corresponds to an uncertainty of the beam positions at the outer field degrader of ± 3.7 mm in x-y direction and ± 2.4 mm in z direction.

5 Alignment and Installation

This section describes the alignment procedures for the mirrors and the support frames, and their installation at the detector.

As described in section 4, the mirrors are mounted on two independent support frames: the distributor wheels outside the detector and the mirror support cones near the jet chamber (figure 2). This concept of support frames instead of mounting all mirrors individually made it possible to align the mirrors beforehand, allowing a fast installation at the detector.

The beam path was set up in the laboratory by simulating the geometrical configuration at OPAL as shown in figure 7a and b. This allowed us to perform a precise and accurate alignment of all mirrors. For the final installation in the detector, only the two support frames as a whole had to be aligned. All mirrors mounted on the support cones inside the jet chamber pressure vessel are not accessible after installation, the distributor wheels are only accessible during LEP shutdowns.

Distributor wheel and mirror support cone were never available at the same time in the laboratory and thus special effort was necessary to define the final beam paths. A special reference disk was constructed for this purpose. Small holes define the nominal beam positions in the r-ϕ plane for all 48 beam paths. These reference holes have a diameter of 4 mm and were drilled with a precision of better than 50 μm. In the final set-up, the distributor wheel is adjusted parallel to the mirror support cone at a distance of 4.4 m. In the laboratory, the reference disk was mounted at the same distance parallel to either the mirror support cone or the distributor wheel, replacing each other. This set-up defined the long straight section of the beam path. The parallelism and the ϕ-angle in the r-ϕ plane were adjusted by means of surveying methods. The allowed tolerances were: $\delta\phi$ better than 9 mrad, $\delta\theta$ better than 1.7 mrad and difference in height of the order of 500 μm. The relative adjustment of the frames was surveyed before and after the mirror alignment. The achieved parallelism of the distributor wheel and the reference disk and their relative difference in ϕ was better than 0.3 mrad.

In a first step, the mirrors and beamsplitters on the mirror support cone were aligned (figure 7a). In this case, the reference disk replaced the distributor wheel defining the nominal

beam positions. For each sector, a laser beam was adjusted to follow the nominal beam path, going through the centre of the reference holes and passing through a 4 mm diaphragm in front of mirror M5 on the mirror support cone. The mirrors were placed in position and adjusted to guide the laser beam along the designed beam path.

The beamsplitters are mounted in their holders together with the last mirror M7, as described in section 4.4. Their nominal ϕ positions were defined by a precision mechanical lever which was rotated for the individual beams. Small deviations of the nominal θ angle were measured (accuracy of 0.1 mrad) and tabulated.

Because of the lack of accessibility to the mirror system once installed on the jet chamber a test mounting of the completed support cone at the jet chamber was done. The mirror support cones were then taken back to the laboratory in order to check all beam paths once again in the same way as described above.

The final accuracy of the azimuthal and polar beam angle with respect to the jet chamber was determined to be 2.2 mrad for ϕ and better than 1.4 mrad for θ.

In a second step, the mirrors on the distributor wheels were aligned together with the main mirror (figure 7b). This time, the reference disk replaced the mirror support cone. The alignment of the mirrors M4 reflecting the beams parallel to the LEP beam axis is in particular critical because of the long distance of 5.4 m to the jet chamber. Since the mirrors M4 are equipped with micrometers, it is possible to do minor corrections of their alignment after installation at the detector.

For facilitation, all alignments were carried out by use of a visible Helium-Neon laser. After alignment of all components, a Nd:YAG beam was passed through the system in order to check all optical surfaces and to measure the beam positions on the beam detectors. After installation of the mirror system at OPAL, these positions were used to steer the laser beam to its nominal positions as described in section 6.

Finally, the distributor wheel and the main mirror were installed at the detector. At that time, the support cones were already mounted onto the jet chamber inside the pressure vessel. A survey was carried out, defining the correct position of the distributor wheel and main mirror. The accuracy achieved was as good as in the laboratory.

In order to allow access to the detector in shutdown periods, the distributor wheel has to be dismounted; usually once per year. Even after the third re-installation of the wheels only three mirrors (M4) showed a small misalignment. A readjustment of these mirrors was always possible by visual inspection and with help of the beam detection system.

6 Beam Detection and Steering

The control system of the laser calibration system is designed to steer the beam into a preselected sector and to handle relevant tasks during data taking. This includes controlling the trigger logic, communication with the jet chamber read-out system and monitoring of system parameters.

All tasks are controlled by microprocessors which allows a high degree of automatization. The microprocessors used are of the 68030 type, operating under the OS9 system in a VMEbus based system [24].

Beam steering is performed by setting the appropriate main mirror position for a given sector and fine tuning of the final beam position using the beam detection system.

The positioning accuracy finally achieved is in the order of 100 μm at the jet chamber entrance window. In addition, the system is designed to cope with contingent small misalignments

or mechanical settlements. To give an example, ramping up the OPAL magnet to its nominal field of 0.435 T leads to a laser beam displacement in the order of 300 μm at the jet chamber and a change in angle of about 0.1 mrad.

In the following sections we describe the beam detection system and our method of steering the laser beams.

6.1 Beam Detection System

The beam detection system is based on position-sensitive detectors. Planar photo diodes are used to measure the laser beam positions and scintillating monitors serve as coarse veto signals. For details on the geometrical position of these detectors see section 4.

The planar photo diodes are of a two dimensional tetra lateral type operated in reversed bias mode [25]. The rectangular sensitive area is 10 mm × 10 mm and is protected by a narrow band optical filter against background radiation [26]. The photo current is collected at thin aluminum strip contacts at the four sides. The charge produced by the incident laser beam is divided according to the resistance from the point of origin to each of the read out sides. Since the resistance of the diode material is homogeneous, resistive charge division is a measure of the beam position on the diode. The normalized charge difference of opposite sides is directly proportional to the spatial coordinate along this direction. However, the geometry of the diode and read out strips leads to non-linear deviations from the simple charge division scheme. The deviation is up to 10 % of the diode length for off centre hits. An iterative correction algorithm was developed to account for this effect [27].

The photo current is converted into a proportional voltage, followed by an integration yielding a measure of the input charge. The read-out electronics has a negligible input resistance to maximize the sensitivity of the position measurements. The measured charge is digitized by a 12-Bit analogue-to-digital converter and read out by the microprocessor.

The precision of the position measurement is in the order of 100 μm (RMS). Since the laser beam position is measured with two beam detectors at a distance of 4.4 m, this number leads to an accuracy of positioning the laser beam of better than 50 μrad.

Scintillating monitors placed around the nominal beam axis at the laser cone increase the sensitive area of beam detection to 500 mm^2. The monitors are divided in four quadrants of scintillating material [28] to give a coarse information of the beam position. The scintillation light induced by the laser beam is measured by small photo diodes [29].

6.2 Beam Steering

The main mirror, the half-wave plate and the telescope are driven by direct current motors. The movements of the devices are measured by incremental angular or linear encoders. The encoders deliver an increment relative to an absolutely fixed reference position. This increment is strictly proportional to the change in angle or distance.

To control the dc motors, we developed special motor control units [30]. The control units steer the devices automatically once the microprocessor has delivered the nominal position. This is done by using the information of the encoders to regulate the motor power and the direction of motion. Depending on the distance to the nominal position, the motor velocity is increased or slowed down. The final position is approached smoothly to avoid regulation oscillations.

For calibration runs, all devices have to be set to their optimal positions. They are different for each beam path. The focal length of the telescope and the half-wave plate angles were

determined beforehand and stored in a table, as well as a set of coordinates for the main mirror (z, y, θ, ϕ). All operations are automated by means of microprocessor control.

To obtain the coordinates for the main mirror after initial installation, the beam is manually steered into a first sector. An automatic procedure scans over the accessible range of the main mirror until signals on the beam detectors are detected. The laser beam is coarsely adjusted, when both planar photo diodes are hit. The accuracy in beam angle is then already better than 2 mrad. The main mirror positions for the next sectors are extrapolated using the known geometry of the beam channels.

Before calibration runs, an additional fine adjustment is done. For this, the laser beam is steered to its nominal positions on the planar photo diodes. They have been determined during the alignment of the system in the laboratory as described in section 5, and have been optimized by checking the quality of the laser induced signals observed in the jet chamber.

A simple and fast algorithm for the fine adjustment was developed. The central task is to translate the laser beam position as measured by the beam detection system to appropriate corrections of the main mirror position.

The four degrees of freedom of the main mirror are expressed in a vector $\vec{m} = (z, y, \theta, \phi)$. In principle, the laser beam is first rotated to be parallel to the nominal beam direction followed by a linear shift to match the nominal position. From the measured positions of the laser beam on the two positioning diodes $(u_i, v_i), i = 1, 2$, the displacement vector $\delta\vec{w} = (\delta u_1, \delta v_1, \delta u_2, \delta v_2)$ is determined. Then the correction vector for the main mirror $\delta\vec{m} = (\delta z, \delta y, \delta\theta, \delta\phi)$ is calculated according to $\delta\vec{m} = R\,\delta\vec{w}$. The 4×4 transformation matrix R depends on geometrical constants only, and is different for each sector. The matrices are calculated from the geometrical position of the main mirror and the planar photo diodes. The fine adjusting procedure has to be repeated iteratively. The desired accuracy of 100 μm is reached within a few iteration steps. A change from one sector to another usually takes less than 5 min.

7 Determination of Calibration Constants with Laser Beams

Since the startup of the LEP machine several complete laser scans of the jet chamber have been performed. The initial calibration was completed in September 1989, just before the first physics run. Data were taken with and without magnetic field for all sectors. Usually about 2000 events are taken per half-sector. The typical time needed to scan through all 24 sectors from both sides is of the order of 24 hours, with the laser running at a repetition rate of 5 Hz. A complete scan is usually performed at the end of each LEP shutdown. In addition data are also recorded for selected sectors, typically every two weeks.

Since the summer of 1991 laser data are also recorded during normal physics runs. In order to keep the induced read-out dead time short the laser repetition rate is reduced to 0.04 Hz. A typical LEP fill lasting for about 10 hours is sufficient to obtain in the new permanent monitoring mode data for one or two jet chamber sectors. In this way the entire chamber can be monitored within a period of two weeks.

The basic methods to obtain calibration constants with laser beams are already described above in section 3.2. In the following we give more details on the methods used and summarize basic results obtained so far.

7.1 Drift Time Determination

The start signal for the laser and the signal to read out the data of the jet chamber are both delivered by the common OPAL trigger signal. The laser light is emitted about 230 μs after

triggering the laser, with a jitter of 100 ns. However, the fast vacuum photo diode delivers a precise time signal of the laser pulse with a time resolution of 100 ps. The time difference between the start of read-out and the actual laser pulse is measured with a time-to-digital converter with a resolution of 250 ps.

The arrival time of the laser induced pulses in the jet chamber is determined from the FADC signals by a timing algorithm developed for laser events (Integral Method [31]). Figure 8a shows the measured drift times of an alternating laser double beam for one wire and figure 8b the time resolution[2] as a function of the wire number. The time resolution achieved is below 1 ns, the mean resolution from wire 2 to 100 in figure 8b is 0.79 ns with a standard deviation of 0.06 ns. Due to diffusion, the resolution decreases for higher wire numbers, where the drift distance is longer.

7.2 Individual Time Offsets

Differences in cable lengths and delays of electronic modules result in relative differences in arrival time of the chamber signals $t_{0,i}$, individual for each wire i. The mechanical staggering and electro-static deflection cause again wire dependent time offsets $t_{stagg,i}$. In general, all measured deviations from a straight line fitted to the laser track are due to these relative time offsets, but in addition also due to inhomogeneities of the drift field.

In order to measure the relative time offsets, two separate laser runs on either side of the anode wire plane are performed. The laser beam angles $\pm\Phi$ with respect to the anode plane are equal to within 3 mrad. This minimizes systematic errors due to slightly different drift lengths and drift fields. The measurement is done with the magnetic field switched off to guarantee an identical drift field configuration on both sides of the anode plane.

By changing the side with respect to the anode plane, the time offsets due to the staggered sense wires $t_{stagg,i}$ change their sign, whereas the individual time offsets $t_{0,i}$ do not. Measuring the residuals from a straight line fit $t_{res,i}$ allows both, $t_{0,i}$ and $t_{stagg,i}$ to be resolved :

$$t_{0,i} = \frac{1}{2}(t_{res,i}(+\Phi) + t_{res,i}(-\Phi)) \tag{1}$$

$$t_{stagg,i} = \frac{1}{2}(t_{res,i}(+\Phi) - t_{res,i}(-\Phi)) \tag{2}$$

The individual time offsets are measured separately for each wire end. As example we show the measured staggering of the signal wires for one sector as a function of the wire number in figure 8c. Shown are the differences in drift time alternating from wire to wire due to the staggering of the sense wires. In this example the mean staggering is $\pm 2.18 \pm 0.19$ ns for both the even and the odd wires. This translates into a mean staggering of $\pm 115 \pm 10\,\mu$m at the position of the laser beam, using a drift velocity of $52.7 \pm 0.04\,\mu$m/ns. The errors given are standard deviations of the relevant distributions.

7.3 Drift Velocity

The drift velocity is obtained by measuring the difference in arrival time of the signals produced by two parallel laser beams with a spacing of 10 mm. In order to avoid systematic corrections

[2]The time resolution for a wire i is defined as $\sigma_t = \sqrt{2/3}\,\sigma_{trip}$, where σ_{trip} is the standard deviation of the triplet distribution. The triplet time t_{trip} is defined as the time difference of the given wire i to the mean of its equidistant neighbours $(i-1)$ and $(i+1)$: $t_{trip} = (t_{(i-1)} + t_{(i+1)})/2 - t_i$.

necessary in the presence of a magnetic field, the measurement is done with the magnetic field switched off. To generate the parallel beams, a monolithic beamsplitter as described in section 4.4 is used. It guarantees high accuracy, stability and reproducibility.

The drift velocity v_D is obtained by measuring the time difference Δt of the double beam signal:

$$v_D = \frac{\Delta s}{\Delta t \cos \Phi} \tag{3}$$

where Δs is the double beam distance, Φ the angle of the laser beam with respect to the anode plane. This angle is known within 2.2 mrad which is well within the accuracy of 10 mrad necessary to obtain a 0.1 % measurement error on v_D.

If both beams are supplied at the same time, the beam nearest to the anode changes the drift field seen by the other beam. The first electrons arriving at the sense wire produce a cloud of ions around the wire after gas amplification. This ion cloud reduces the gas amplification close to the sense wire [32] and leads to a temporary distortion of the drift field. This results in a systematic error in the drift time measurements. In order to avoid such a space charge effect, an alternating beam method has been developed [33].

The linear polarization of the laser beam, together with the special coating of the beamsplitters, are used to obtain the alternating beam as illustrated in figure 9. If the laser beam is polarized normal to the incident plane (s-polarization), the beam nearest to the anode plane (beam 1) is suppressed. The ratio of intensity in the chamber response of beam 1 to beam 2 is better than 1:100. A laser beam polarized parallel to the incident plane (p-polarization) suppresses the beam furthest from the anode plane (beam 2). The beam suppression of beam 2 to beam 1 is approximately 1:9, which is sufficient in this case.

The orientation of the polarization vector at the beamsplitters is adjusted by means of the half-wave plate near the laser. The half-wave plate rotates the orientation of polarization to be either normal or parallel. The Pockels cell, mounted between the laser and the half-wave plate, switches the polarization state. The Pockels cell is used to rotate the orientation of the laser beam polarization by 90°. This allows the polarization state to be switched and thus enables alternation between near and far anode laser beams shot by shot. The repetition rate may be up to 10 Hz.

The drift velocity for one sector is shown in figure 10a as a function of wire number. The mean drift velocity in this example is $52.69 \pm 0.04\,\mu$m/ns. The error is given as the standard deviation for the drift velocities from wire 20 to 140. The variations in drift velocity at the inner and outer wires are due to inhomogeneities of the drift field (see section 7.5).

Figure 10b shows the drift velocity as a function of jet chamber sector number. The drift velocity was found to be independent of the sector. Figure 11 shows the drift velocity monitored over an extended time period. For comparison, a measurement of the water content in the jet chamber gas is also shown in the same plot [34]. It is evident, that the observed variations in the drift velocity were mainly due to the small changes of the water content. Usually the water content is kept stable at 500 ppm within $\pm$25 ppm.

7.4 Lorentz Angle

The OPAL magnetic field of 0.435 T results in a rotation of the effective drift path of the electrons by the Lorentz angle, α_L, which is about 20° (figure 1a). Thus, the angle of the drift cell with respect to the laser beam is $\alpha_L \pm \Phi$. Here Φ again is the angle of the laser beam with respect to the anode plane, the sign depends on the side relative to the anode. Measuring the

drift time difference of the double beam Δt^B allows the Lorentz angle to be determined :

$$cos(\alpha_L \pm \Phi) = \frac{\Delta s}{v_D^B \Delta t^B} \tag{4}$$

where Δs is the double beam distance as measured in the laboratory and v_D^B the drift velocity in presence of the magnetic field. Counting only the statistical errors, the Lorentz angle can be measured with a precision of better than 1 %. However a systematic uncertainty of this method arises from the fact that the drift velocities with and without magnetic field are not exactly equal [35]. For the jet chamber this ratio was estimated from laser measurements to be about 0.25 % above 1.

Since the systematic uncertainty of the drift velocity in the magnetic field is still of the order of 0.2 %, the absolute knowledge of the Lorentz angle is not better than 1.5 %. Work is in progress to determine the ratio of drift velocities with and without magnetic field in the order of 0.1 % to achieve an accuracy on the measurement of the Lorentz angle of 1 %.

The Lorentz angle as function of wire number is shown for a selected sector in figure 12a. In this plot a drift velocity ratio of 1 was used. Also shown is a distribution of the Lorentz angle for wires 20 to 140 in the homogeneous part of the drift field (figure 12b). The mean Lorentz angle in this example is $\alpha_L = 19.74° \pm 0.25°$. The error given is the standard deviation. Again, variations in Lorentz angle at the inner and outer wires are due to inhomogeneities of the drift field (see section 7.5).

7.5 Drift Field Correction

After the determination of the individual time offsets, all residual deviations from a straight laser track are due to non-perfect knowledge of the sense wire positions or distortions of the electric field.

The electric field of the OPAL jet chamber is homogeneous over almost the whole chamber volume. However, small field distortions at the innermost and outermost wires could not be completely eliminated, although the design of the cathodes and field shaping electrodes minimizes these distortions.

The residuals as a function of wire number are shown in figure 13 for measurements without magnetic field (13a) and with the nominal magnetic field of 0.435 T (13b). Small deviations from a homogeneous field at the inner and outer radius of the chamber are visible. The deviations at the outer wires change by up to 30 ns when the magnetic field is switched on.

These measurements are used to adjust one parameter describing the field inhomogeneity caused by the outer field shaping electrodes. With the help of a field calculation program, a parametrization of field distortions was developed, including the regions not accessible to the laser.

7.6 Systematic Sagitta

The finite momentum resolution for particle tracks is due to the spatial resolution, remaining systematic effects, and the contribution due to multiple scattering. The systematic errors can be expressed in terms of a residual sagitta of a perfectly straight laser track.

We determine the residual sagitta of a laser track by applying a parabola fit, after correction of all known effects like individual time offsets, staggering, field inhomogeneities, and other corrections. The parabolic term is a direct measure of the remaining systematic sagitta. A

systematic shift of the average sagitta determined with laser tracks would indicate a non-perfect calibration.

Figure 14 shows the residual sagitta of laser tracks after applying all known calibration constants. The mean sagitta observed is 9 μm with a standard deviation of 13 μm. This is in agreement with the expected contribution to the sagitta due to the time resolution alone, which is in the order of 13 μm [36]. From this measurement we conclude, that only a small systematic sagitta is expected for particle tracks in the jet chamber.

7.7 Relative Gain and Effective Wire Length

The coordinate of particle tracks along the sense wires, the z coordinate, is determined by resistive charge division. The charge deposit on the sense wire is divided according to the ratio of resistances at the two ends of the wire. This ratio is a function of the position along the wire. Thus, the measurement of the charges Q_1 and Q_2 at both sense wire ends allows the determination of the z coordinate:

$$z = \frac{l_{eff}}{2} \frac{gQ_1 - Q_2}{gQ_1 + Q_2} \tag{5}$$

The effective wire length l_{eff} and the relative gain g, are calibration constants that are determined individually for each wire. The relative gain is defined as the ratio of the gains at the two ends of the wire. It reflects possible small differences in amplification and pulse attenuation at the two sides of the read-out chain. The effective wire length depends on the impedance of the wire and the preamplifier.

Since there are two unknown constants, one needs at least two laser measurements at different z positions. In a first step, the relative gain g is determined by an iterative procedure, adjusting gQ_1 to be equal to Q_2 according to the ratio of the known z coordinates of both laser tracks. Here, the ratio of the two measured z coordinates is evaluated using the mean z coordinate of the laser track sample rather than the mean charges. The procedure starts with the most probable value of the relative gain $g = 1$, meaning equal amplification at both read-out sides. In a second step, the effective wire length l_{eff} is determined from the known z positions of the laser beams, being a mere scale factor.

However, since the effective wire length turns out to be a function of the actual pulse shape and therefore is a function of the track angle in θ and in Φ, the value obtained here is only exact for the given laser track angles and pulse shapes. Correction factors have to be applied to obtain the final z coordinates for particle tracks.

The effective wire length as a function of wire number is shown in figure 15 (dots). A systematic periodic structure is visible which is due to an electronic modulation of the relative preamplifier gains or of the termination boards. This structure is found to be the same for each sector. For the determination of true z coordinates it is important to incorporate this effect. For comparison, the same figure shows also the theoretical effective wirelength as calculated from the impedance of the read-out chain (solid line), and the pure geometrical wire length (dotted line). The increase of the wirelength with rising wire number is due to the conical end plates of the jet chamber.

7.8 Torsion of Wire Planes

As a final example for the excellent accuracy which can be achieved with a laser system, the measured torsion between the two end flanges of the chamber is shown in figure 16.

The measurement of the residual curvature of the laser beam at different polar and azimuthal angles θ and ϕ allows the basic geometrical constants for a possible torsion of the end flanges and a residual curvature of the anode plane to be determined.

A relative torsion of the end flanges of the chamber leads to systematic displacements of the sense wire planes which depends on z. They have been detected by a θ-scan. The measurement of the geometry was performed during the initial stand alone test of the OPAL jet chamber in fall 1988. In this test it was possible to measure at various laser beam angles, whereas in the final system the laser beam angles are fixed.

The torsion was found to be 100 μm in ϕ at the outer radius of the end flanges corresponding to an angle of 50 μrad. This accuracy could not be achieved by surveying the chamber with conventional optical devices.

8 Summary

In this report a calibration system based on the use of ultraviolet laser beams for the central tracking chamber of the OPAL detector at LEP is described. New methods were developed for the calibration of very large drift chambers. Their principles are explained and the obtained results are presented.

Since the startup of the LEP machine several complete laser scans of the jet chamber have been performed. The initial calibration was completed in September 1989, just before the first LEP physics run. Since then, data has been taken for selected sectors typically every two weeks. Since summer 1991 laser data are recorded during normal physics runs.

In general the experience with the laser system has been very satisfactory, and it was used in many cases to reduce systematic uncertainties. All individual results of the laser measurements contribute to the excellent performance of the OPAL jet chamber. The system has also turned out to be very useful to find hardware or electronic failures in the jet chamber readout chain.

Laser beams have been shown to be a powerful tool for fast and reliable calibration and monitoring.

Acknowledgements

The successful construction of the laser system would not have been possible without the dedicated work done in the workshops at CERN and at the Bonn Institute. We thank Dr. T. Wyatt for carefully reading the manuscript. We gratefully acknowledge the financial support of the Bundesministerium für Forschung und Technologie, FRG.

References

[1] OPAL Collaboration, K.Ahmet et al., Nucl. Instr. and Methods **A305** (1991) 275-319.

[2] R. D. Heuer and A. Wagner, Nucl. Instr. and Methods **A265** (1988) 11-19.
H. M. Fischer et al., Nucl. Instr. and Methods **A283** (1989) 492-501.

[3] H. J. Hilke, Nucl. Instr. and Methods **A252** (1986) 169-179.

[4] H. M. Fischer et al., Nucl. Instr. and Methods **A252** (1986) 331-342.

[5] P. v. Walter and G. Mildner, IEEE Trans. Nucl. Sci. **NS-32** (1985) 626-630.

[6] H. Anderhub, M. J. Devereux, P.-G. Seiler, Nucl. Instr. and Methods **166** (1979) 581-582.
H. Anderhub, M. J. Devereux, P.-G. Seiler, Nucl. Instr. and Methods **176** (1980) 323-324.
H. J. Hilke, Nucl. Instr. and Methods **174** (1980) 145-149.

[7] J. Bourotte, B. Sadoulet, Nucl. Instr. and Methods **173** (1980) 463-470.
M. DeSalvo, R. DeSalvo, Nucl. Instr. and Methods **201** (1982) 357-360.
C. Raine, K. W. D. Ledingham, K. M. Smith, Nucl. Instr. and Methods **217** (1983) 305-310.
J. W. Cahill et al., J. Phys. B **19** (1986) 1989-1996.

[8] This analysis was carried out by L. Stieglitz, Institut für heiße Chemie, Kernforschungszentrum Karlsruhe, July 1985.

[9] The gas is circulated through a chemical filter of the activated copper type (BASF R311) in order to remove oxygen. To keep the water content constant within ± 25 ppm a molecular sieve (3 Å) is added in parallel to the gas volume.

[10] Mini-Q Nd:YAG laser, Lumonics Ltd., Rugby, England.

[11] Pikosecond Vacuum Photodiode TF 1850, Instrument Technology Limit., St. Leonards on Sea, Sussex, England.

[12] KD*P, Model LM 8, Gsänger Opt. Komp. GmbH, Planegg, Germany.

[13] Halle Optische Werkstätten, Berlin, Germany.

[14] Heidenhain AG, Wallisellen, Switzerland.

[15] EG & G Reticon RL 1024 H, Sunnyvale, California.

[16] BK 7 supplied by Wisag AG, Zürich, Switzerland.

[17] Suprasil I supplied by Wisag AG, Zürich, Switzerland.

[18] Laseroptik GmbH, Garbsen, Germany.

[19] Faulhaber GmbH, Schönaich, Germany.
Minimotor, Agno, Switzerland.

[20] Föhrenbach GmbH, Löffingen Unadingen, Germany.

[21] Physik Instrumente GmbH, Waldbronn, Germany.

[22] The 96 micrometers were machined in the CERN workshop and have a resolution of 0.5 mm per turn.

[23] CCD chip from Thomson TH 7882, München, Germany; Camera body and electronics from Kappa Messtechnik, Gleichen, Germany

[24] MC 68030 32 bit Microprocessor, Motorola Inc.
OS9 Operating System for the 68000 processor family, Microware Systems Corp., Des Moines, Iowa.
VME, IEEE 1014/D1.0.

[25] SC-10 D, United Detector Technology, Hawthorne, California.

[26] Optical Filter UG 11, Schott Schleifer AG, Feldbach, Switzerland

[27] J. Koch, Diploma Thesis, Bonn University, BONN-IR-90-12, March 1990.

[28] NE110, Scintillator from Nuclear Enterprises, Edinburgh, Scotland.

[29] BPW 34 B, Siemens-Albis SA, Renens, Switzerland

[30] A. Eyring, S. Gross, Internal Report, Bonn University, 1990.

[31] A. Michels, Diploma Thesis, Bonn University, BONN-IR-86-03, 1986.

[32] J. Va'vra, Nucl. Instr. and Methods **225** (1984) 13-22.

[33] M. Hauschild, PhD Thesis, Bonn University, BONN-IR-88-57, November 1988.

[34] The measurement of the water content was done by P. Igo-Kemenes. For details see also [2].

[35] B. Schmidt, Diploma Thesis, Heidelberg University, 1980.

[36] R. L. Gluckstern, Nucl. Instr. and Methods **24** (1963) 381-389.

Figure Captions

Fig. 1: Position of the laser beams: a) r-ϕ view of a part of one jet chamber sector; also indicated is the rotation of the drift cells by the Lorentz angle α_L. b) r-z view of the OPAL central detector.

Fig. 2: Top view of the experimental area giving an overview of the locations of the components of the laser system.

Fig. 3: The laser and optical components as mounted on the optical bench in the laser cabin.

Fig. 4: The main mirror consists of three individual mirrors: the stationary mirror M1, mirror M2, which is movable along the y axis, and mirror M3, which can be moved in the z direction and can be rotated in polar angle θ and azimuthal angle ϕ.

Fig. 5: a) The distributor wheel is shown in a view along the LEP machine beam axis. Indicated are the different laser beam paths and the locations of the mirrors M4 and M4'. Also shown are the contours of the LEP mini β magnet and the Helium-Neon lasers. b) A detailed side view of one individual mirror mount. These mirrors are equipped with micrometers to allow the adjustment in the angles θ and ϕ as indicated.

Fig. 6: a) The mirror support cone in a cross section parallel to the LEP machine beam axis. b) A photo of a unit before installation on the jet chamber. c) An exploded view of the holder which carries the beamsplitter and mirror M7.

Fig. 7: Laboratory setup for the mirror alignment. Shown are the geometrical configurations for the alignment a) of the mirror support cone, and b) of the distributor wheel.

Fig. 8: a) Drift time distribution for one wire. The two peaks arise from the laser double beam. The double beam distance is 10 mm. b) Time resolution for one sector as a function of wire number. The average resolution is better than 1 ns. c) Sense wire staggering for one sector as a function of wire number. Shown are the measured time differences due to the geometrical and electro-static staggering of the sense wires.

Fig. 9: Method of laser beam splitting. Shown are the beam paths through the splitter for a) normal polarized and b) parallel polarized laser light. Also shown are the resulting pulse shapes as registered by the FADC.

Fig. 10: a) Drift velocity as a function of wire number. b) Drift velocity as a function of sector number. The drift velocity is measured to be independent of azimuthal angle ϕ in the jet chamber.

Fig. 11: Drift velocity monitoring over an extended time period. The solid line gives the result of the monitoring of the water content in the chamber gas. A clear correspondence is observed indicating the dependence of drift velocity on the water content.

Fig. 12: a) Lorentz angle as a function of wire number. b) Mean Lorentz angle for one sector.

Fig. 13: Residuals from a straight line fit to the laser beam after correction of individual time offsets as a function of wire number a) without magnetic field and, b) inside the magnetic field of 0.435 T.

Fig. 14: Residual sagitta of laser tracks after correcting with all known calibration constants.

Fig. 15: The measured effective wire length for one sector is shown as a function of wire number (dots). The solid line shows the theoretical expectation, and the dashed line the geometrical wire length.

Fig. 16: Residual sagitta per sector as a function of polar angle θ. The solid line is a fit to the data indicating a relative torsion of the jet chamber end flanges of 100 μm at the outer radius.

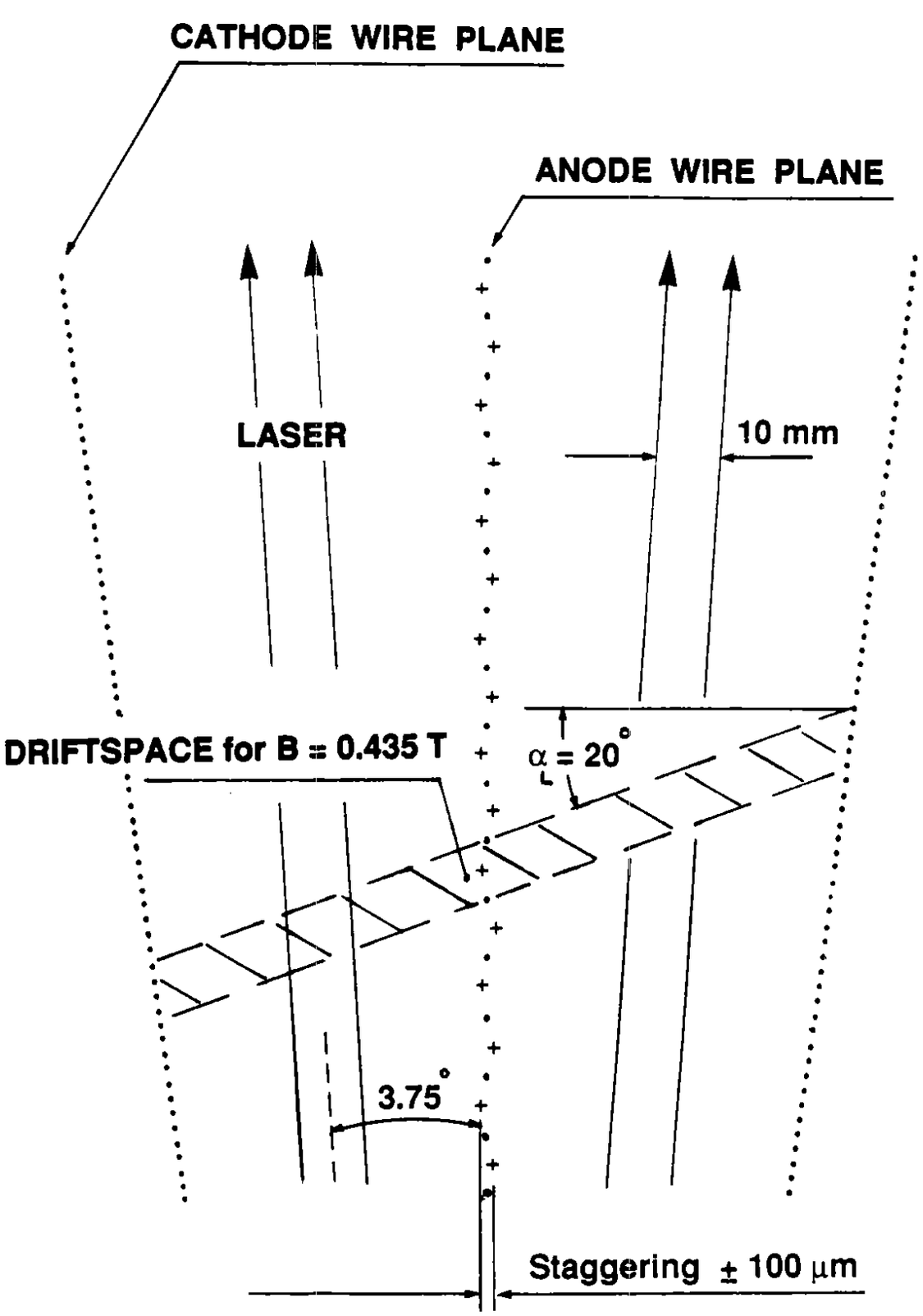
CATHODE WIRE PLANE
ANODE WIRE PLANE
LASER
10 mm
DRIFTSPACE for B = 0.435 T
$\alpha_L = 20^\circ$
3.75°
Staggering ± 100 μm

Fig. 1 a)

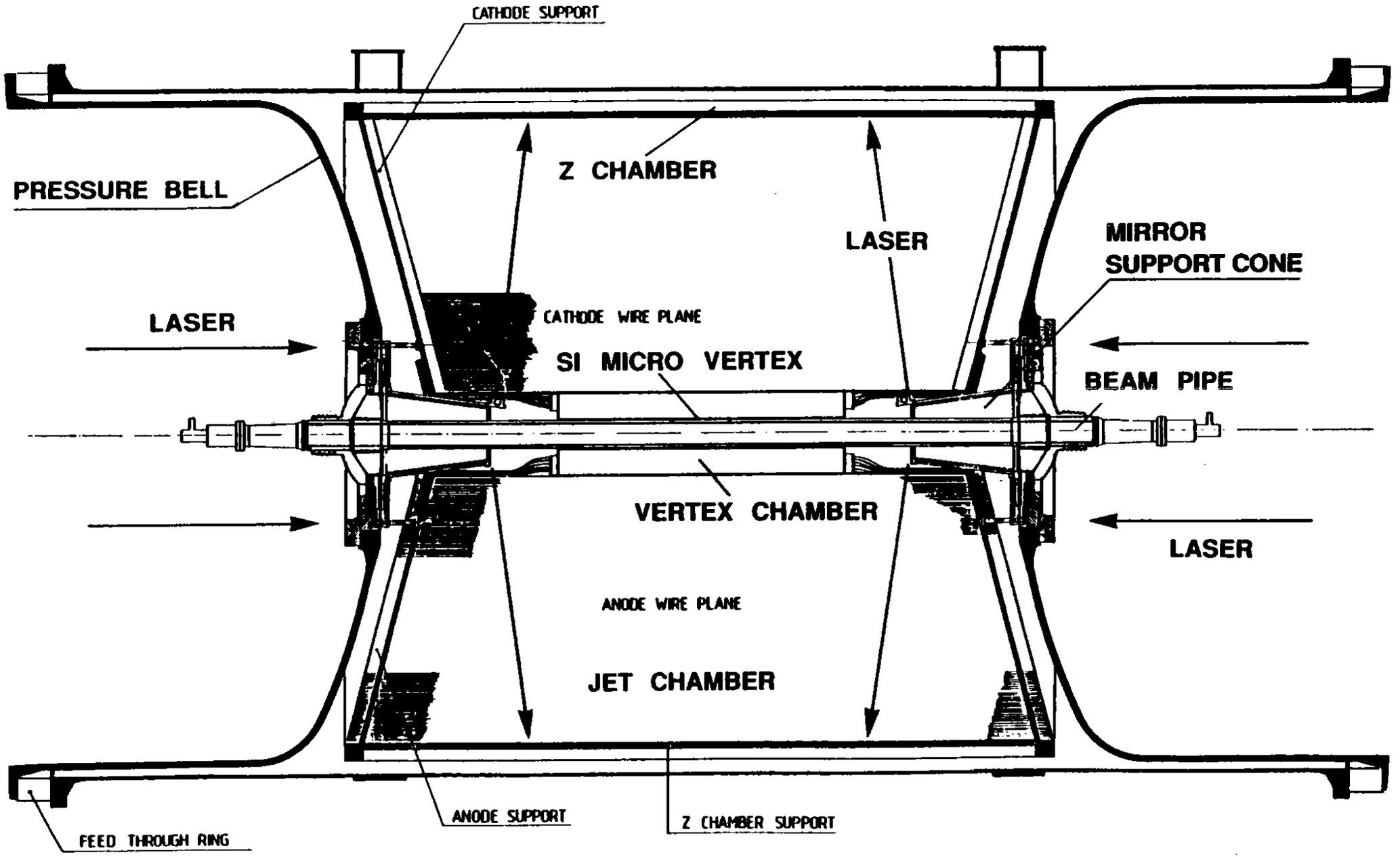

CENTRAL DETECTOR OPAL

Fig. 1 b)

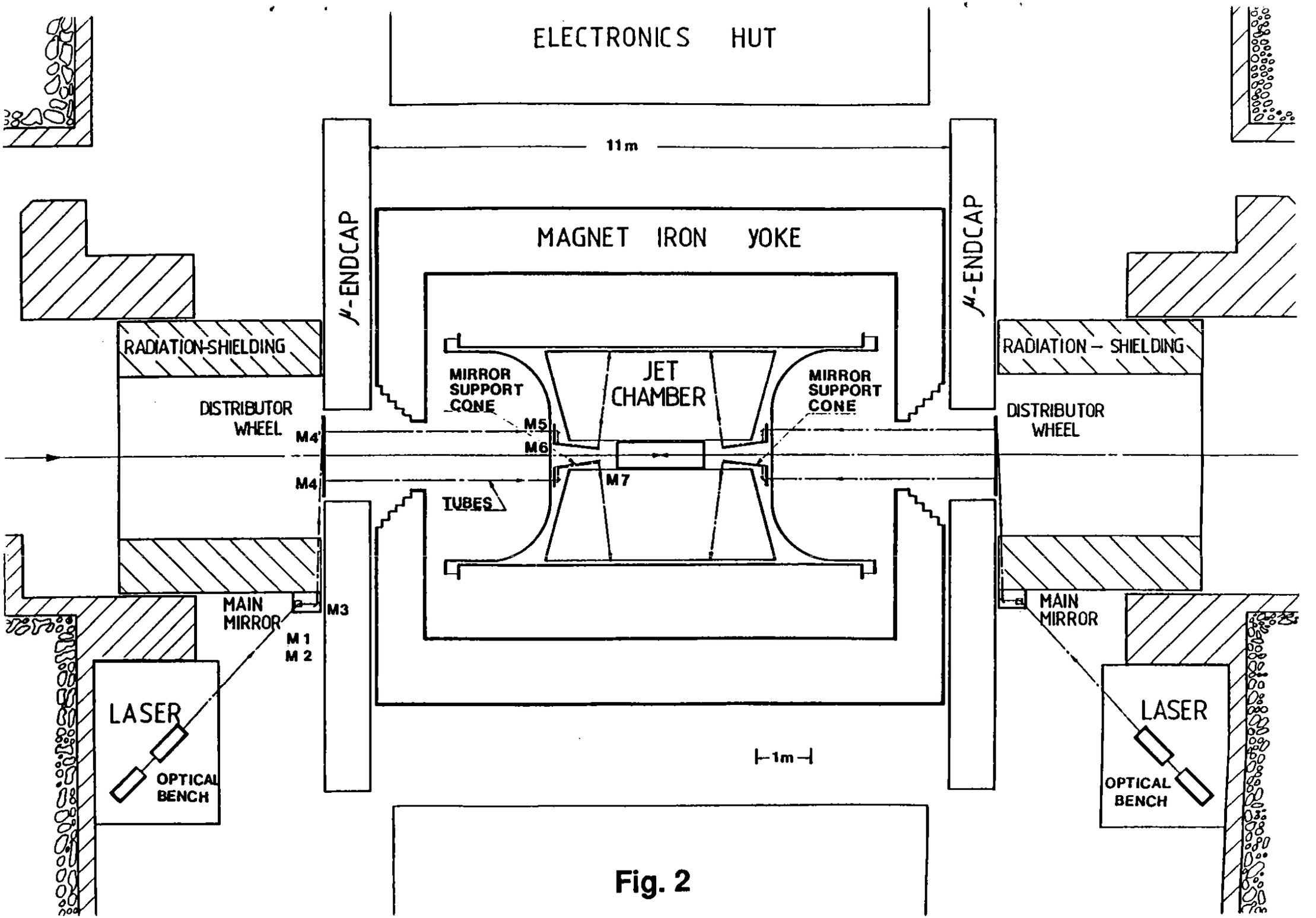
ELECTRONICS HUT
11m
μ-ENDCAP
MAGNET IRON YOKE
μ-ENDCAP
RADIATION-SHIELDING
RADIATION – SHIELDING
MIRROR SUPPORT CONE
JET CHAMBER
MIRROR SUPPORT CONE
DISTRIBUTOR WHEEL
DISTRIBUTOR WHEEL
M4'
M5
M6
M4
M7
TUBES
MAIN MIRROR
M3
M1
M2
MAIN MIRROR
LASER
OPTICAL BENCH
LASER
OPTICAL BENCH
1m

Fig. 2

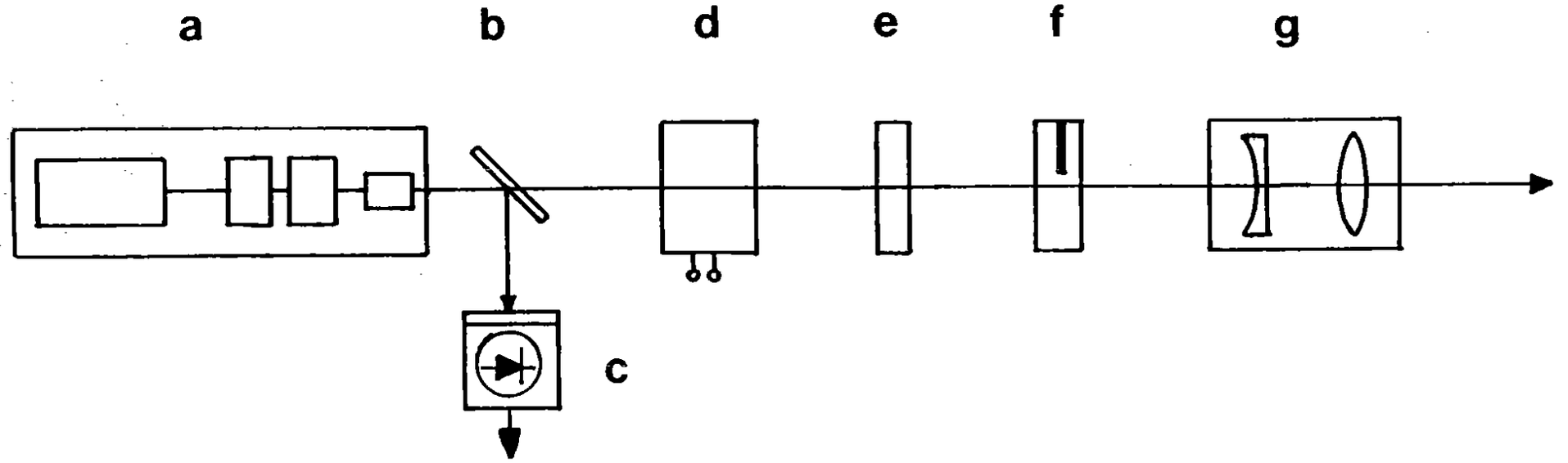

a) Nd : YAG Laser with Frequency Doublers and Wave Length Separator
b) Quartz Plate
c) Fast Vacuum Photo Diode
d) Pockels Cell
e) Half-Wave Plate
f) Beam Shutter
g) Telescope (f = 13 m)

Fig. 3

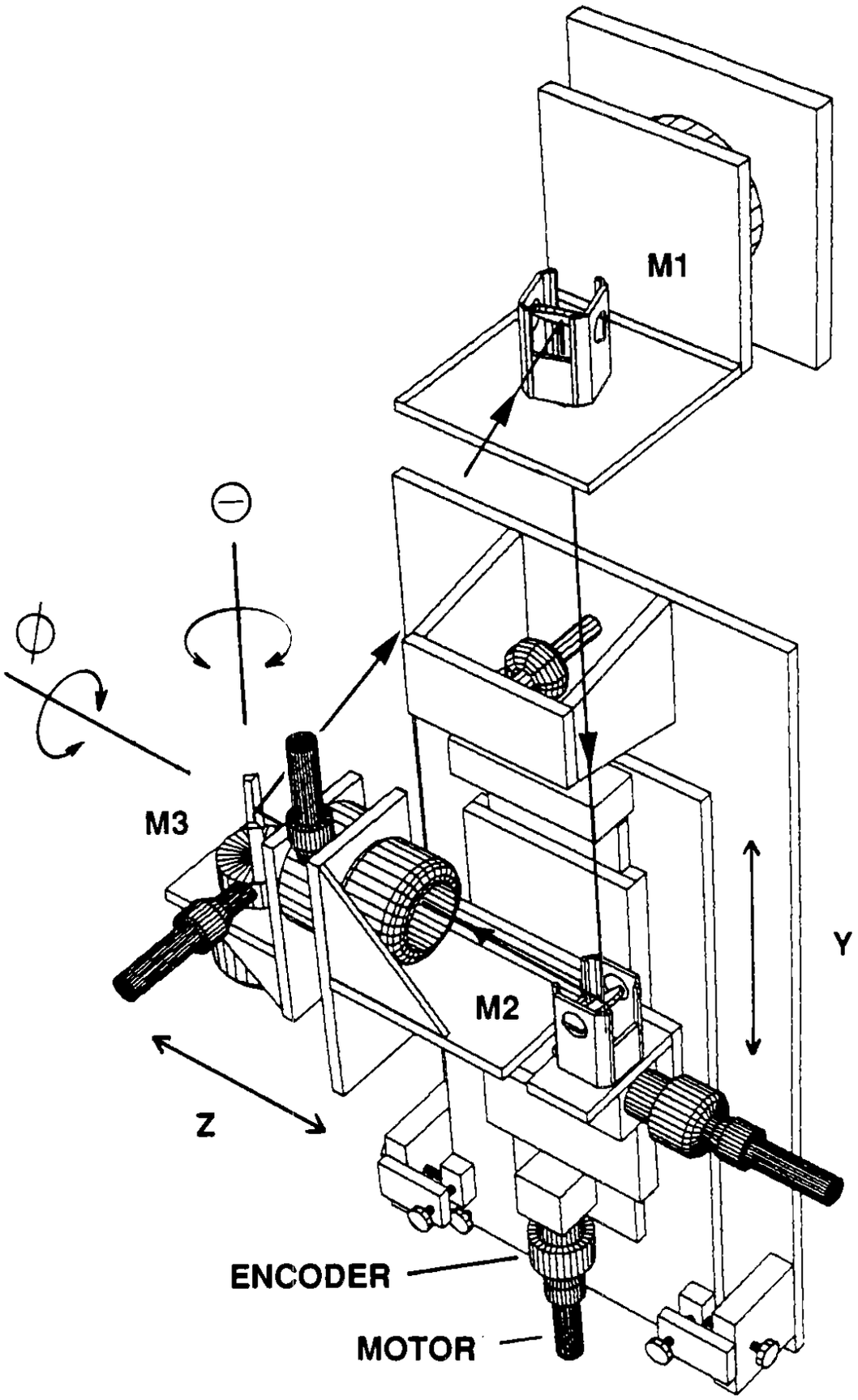

Fig. 4

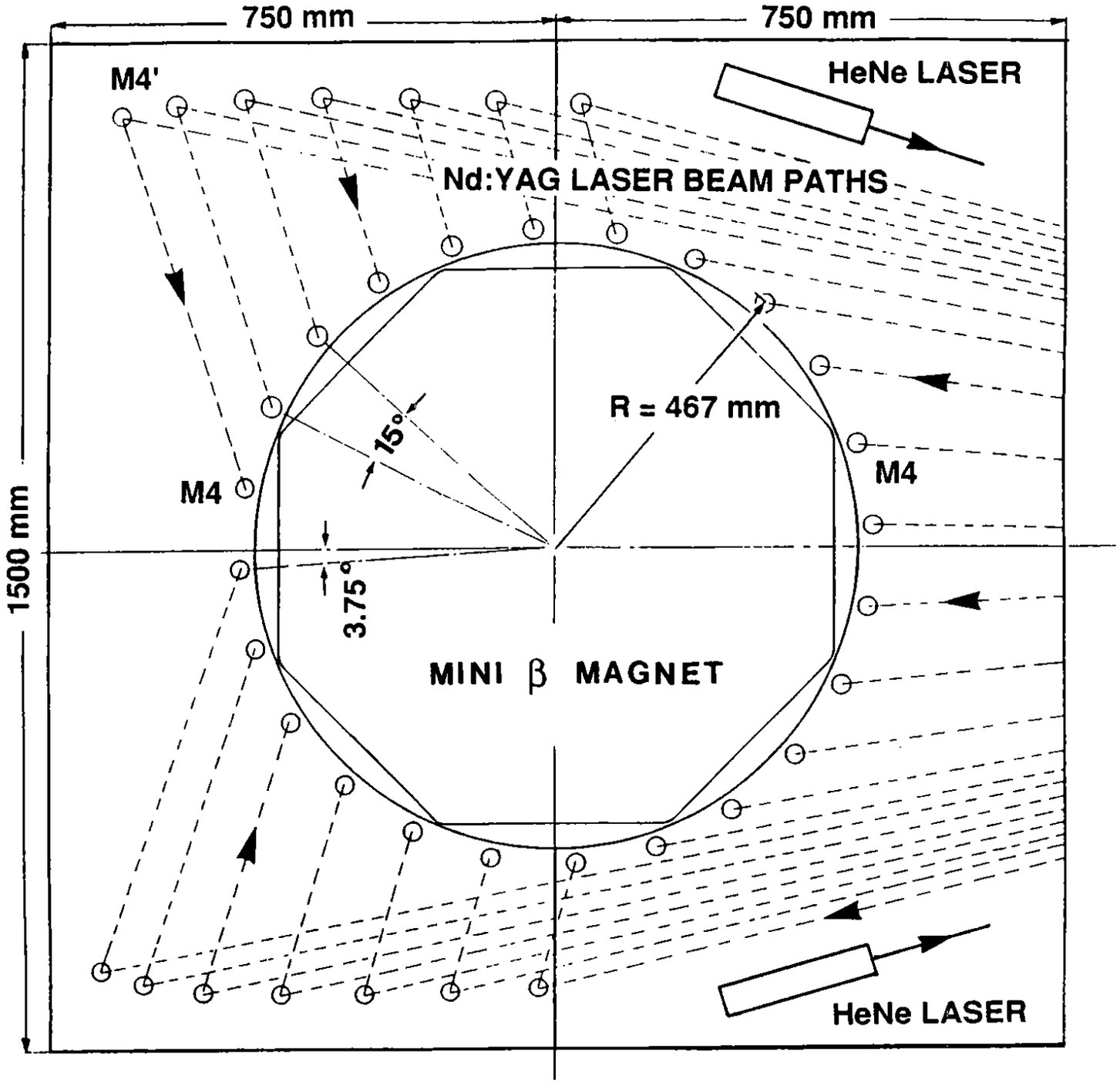
750 mm
750 mm
M4'
HeNe LASER
Nd:YAG LASER BEAM PATHS
R = 467 mm
15°
M4
M4
1500 mm
3.75°
MINI β MAGNET
HeNe LASER

Fig. 5 a)

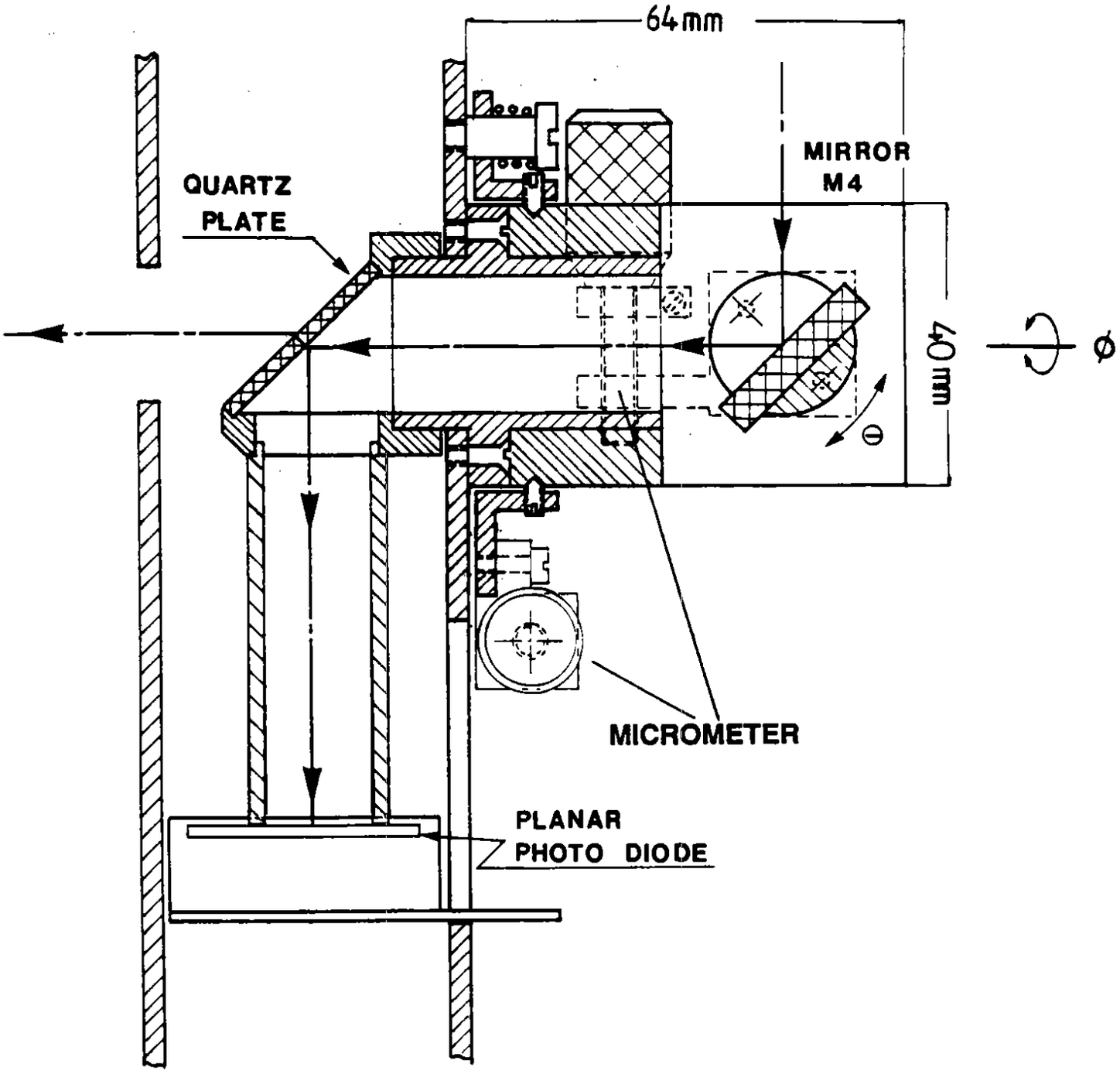
64mm
MIRROR
M4
QUARTZ
PLATE
40 mm
Θ
Ø
MICROMETER
PLANAR
PHOTO DIODE

Fig. 5 b)

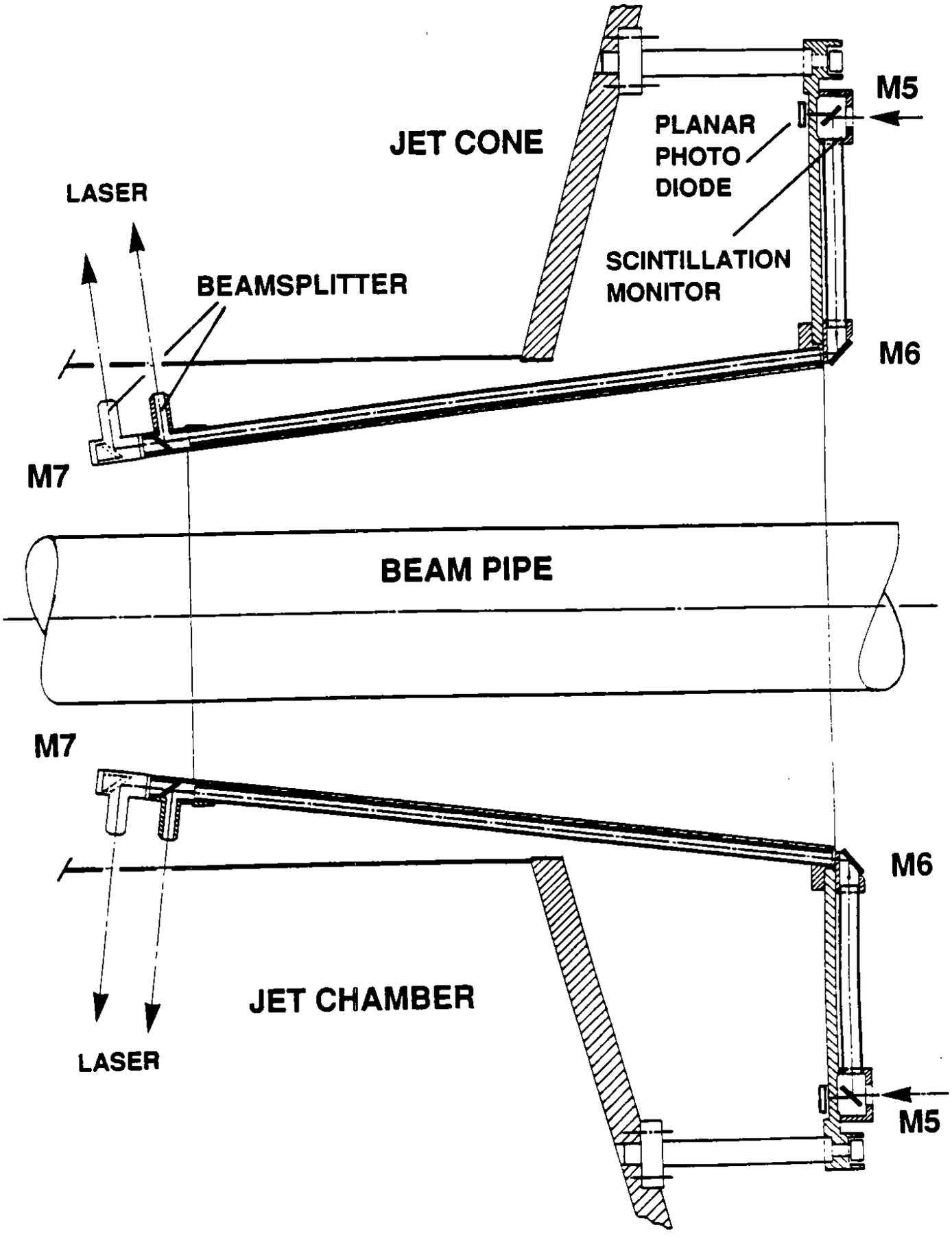
JET CONE
M5
PLANAR
PHOTO
DIODE
LASER
SCINTILLATION
MONITOR
BEAMSPLITTER
M6
M7
BEAM PIPE
M7
M6
JET CHAMBER
LASER
M5

Fig. 6 a)

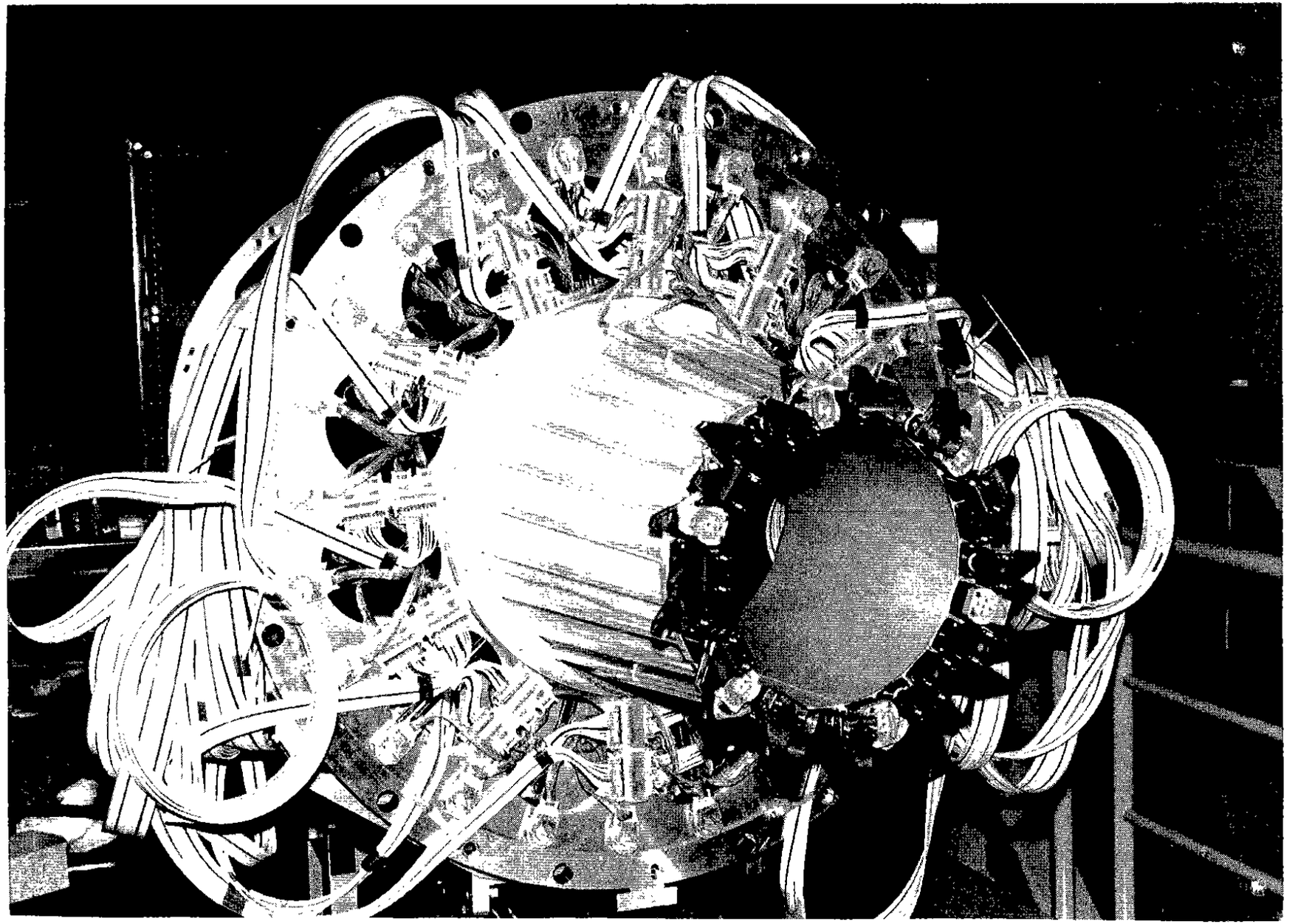

Fig. 6 b)

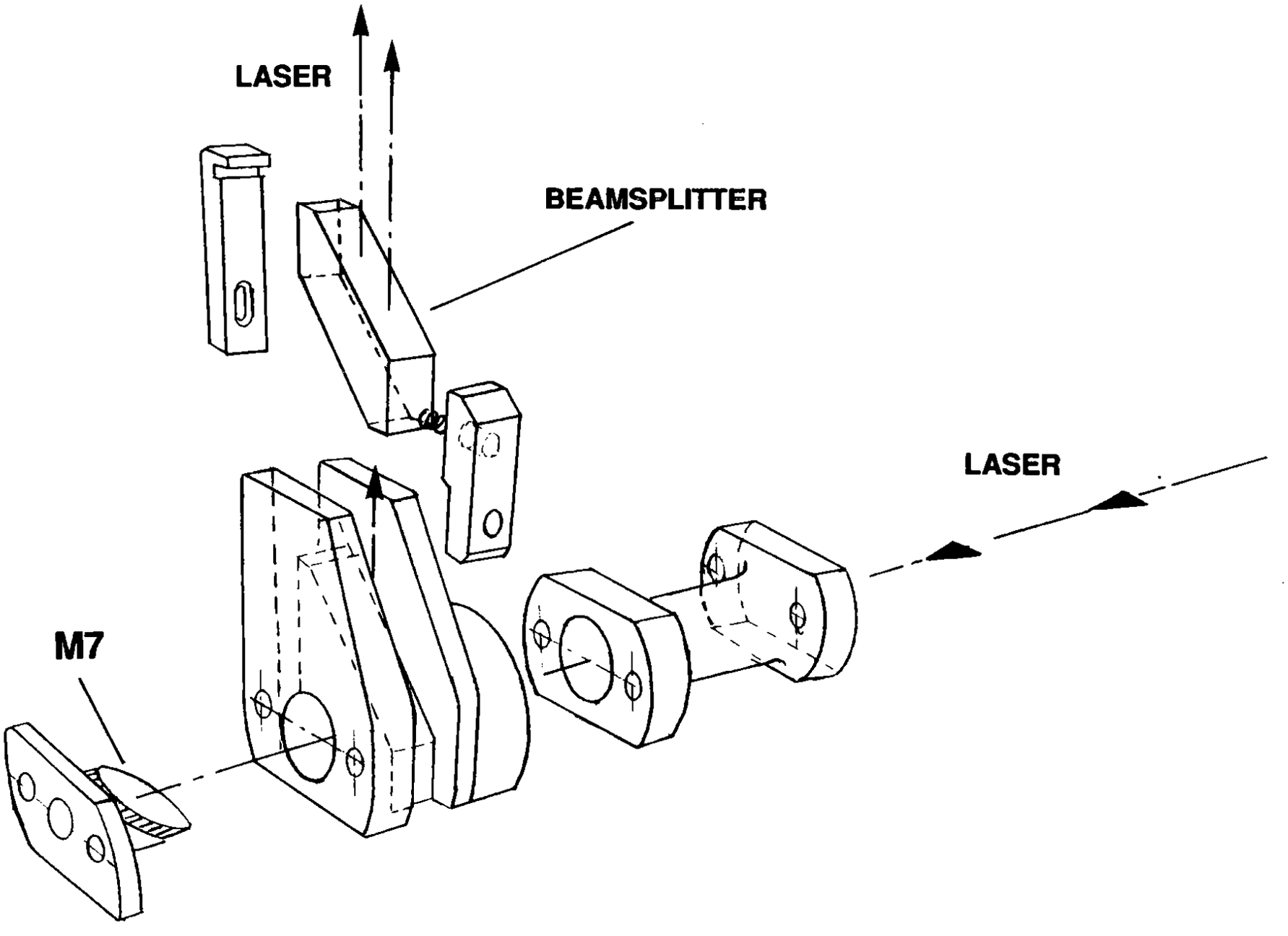

Fig. 6 c)

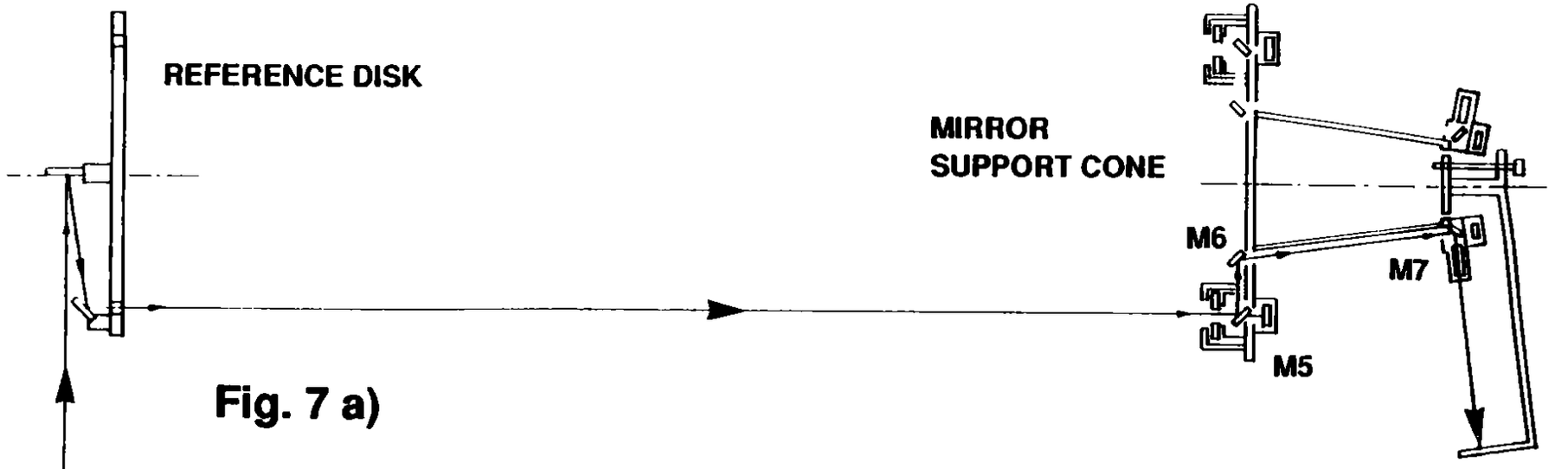
REFERENCE DISK
MIRROR
SUPPORT CONE
M6
M7
M5

Fig. 7 a)

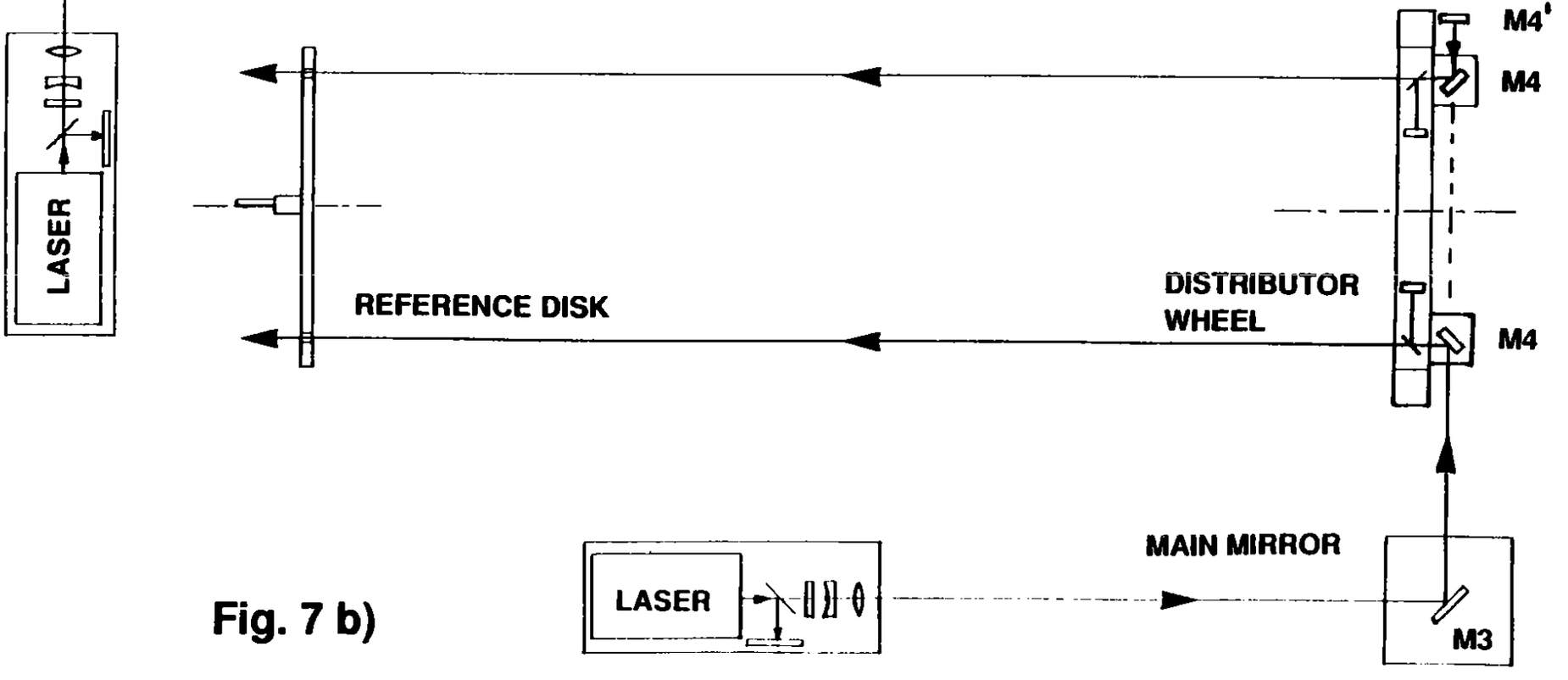
M4'
M4
LASER
REFERENCE DISK
DISTRIBUTOR
WHEEL
M4
MAIN MIRROR
LASER
M3

Fig. 7 b)

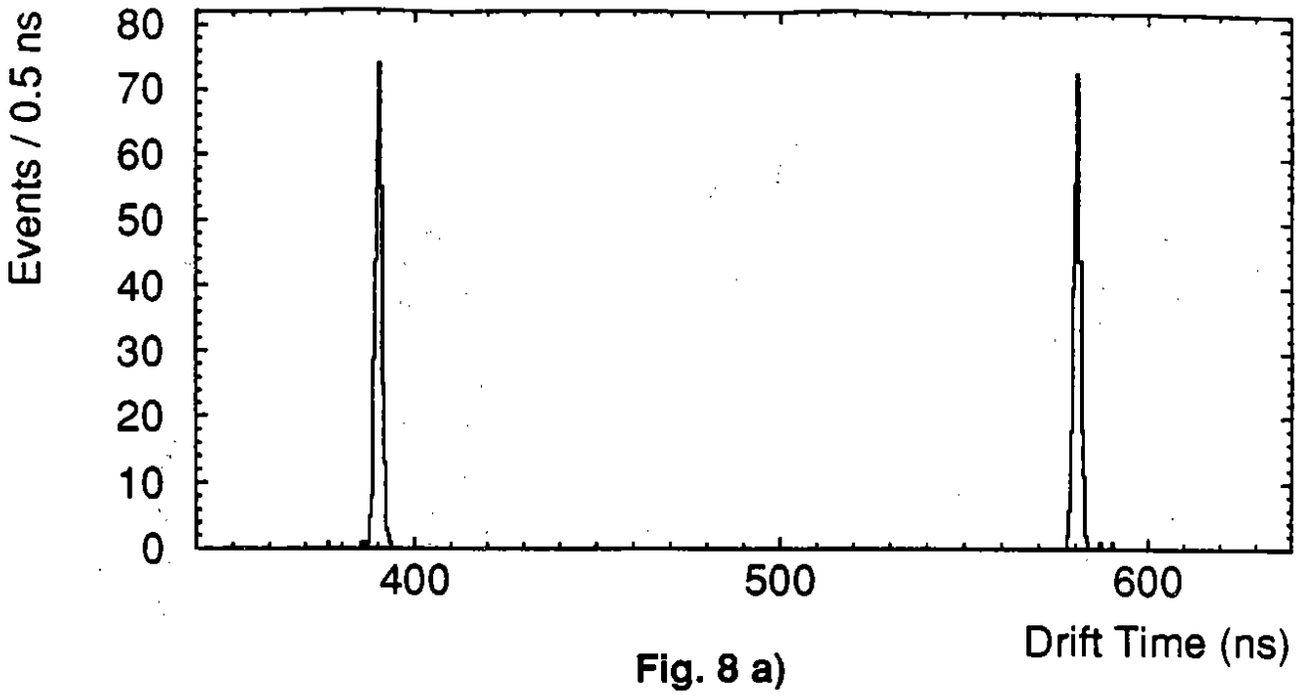

Fig. 8 a)

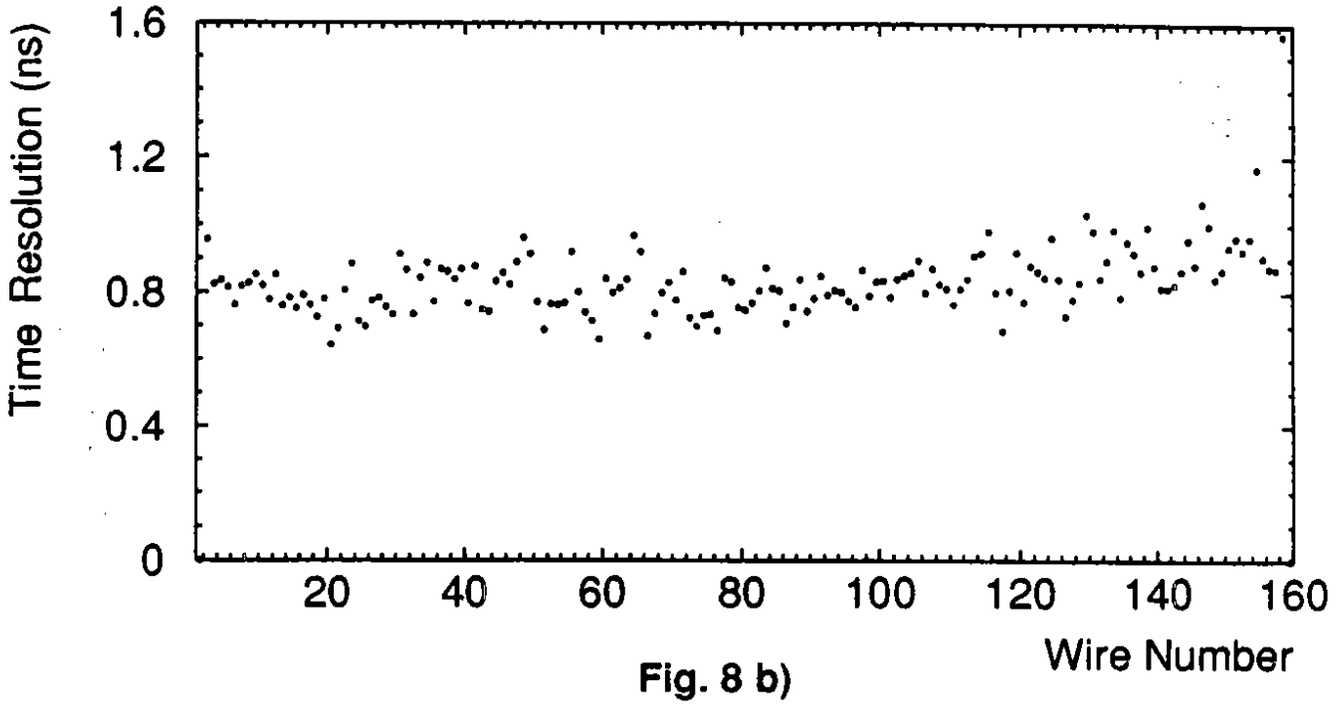

Fig. 8 b)

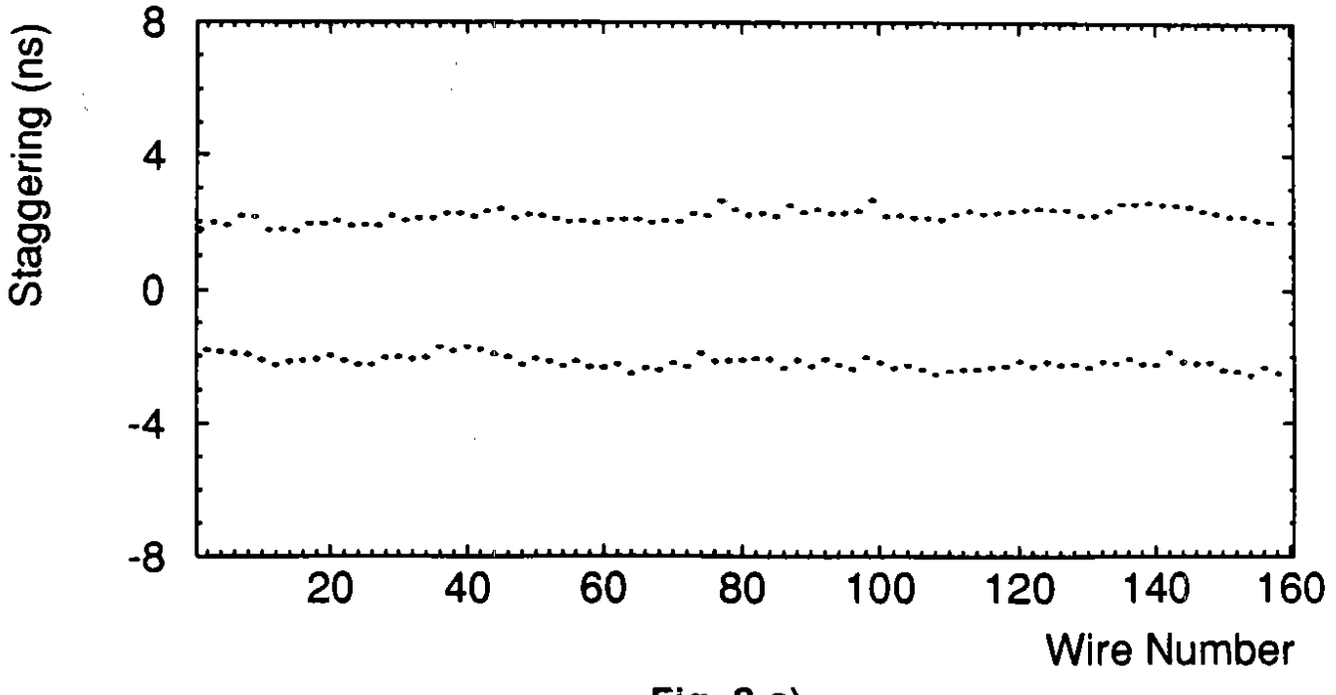

Fig. 8 c)

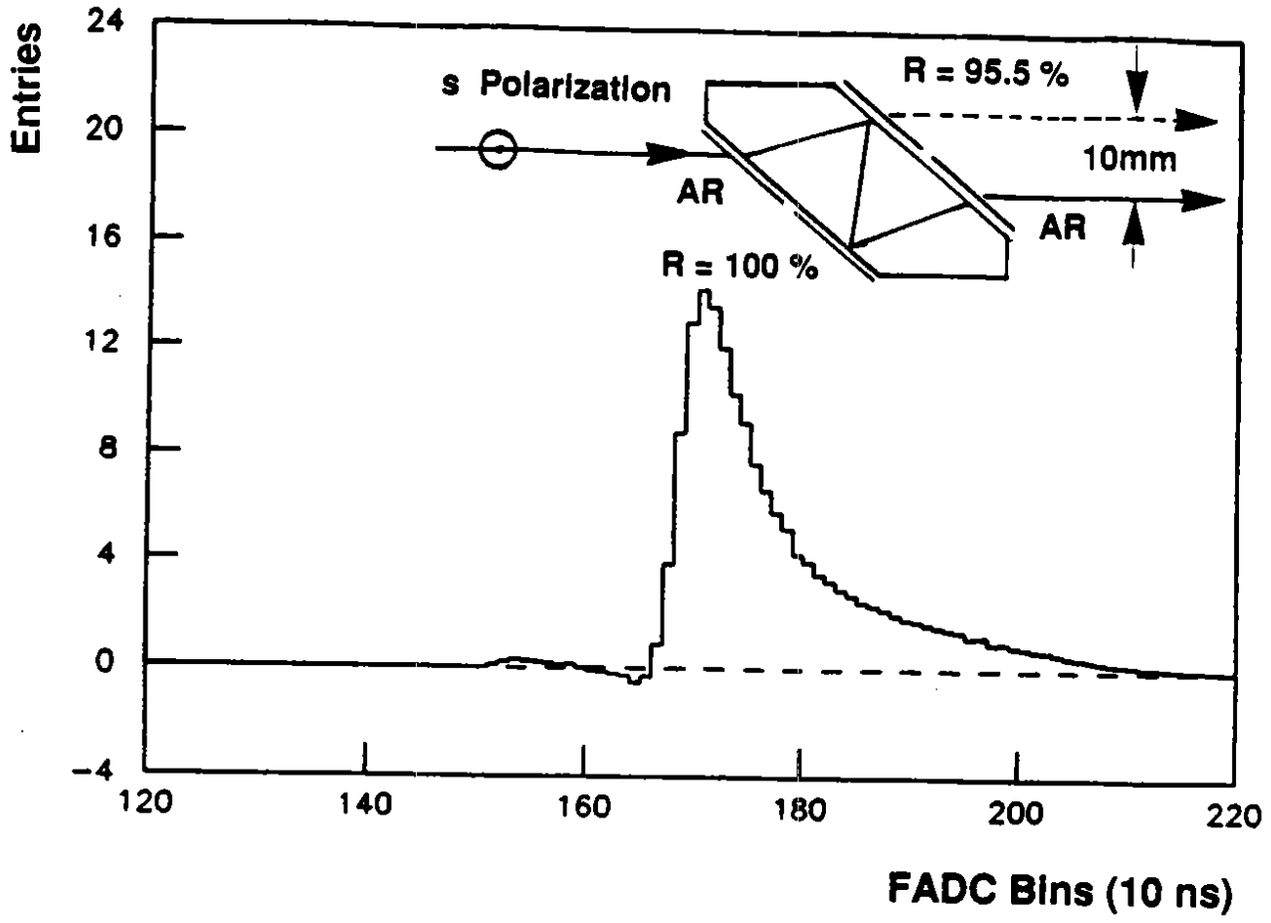
Entries
24
20
16
12
8
4
0
-4
120
140
160
180
200
220
s Polarization
R = 95.5 %
10mm
AR
AR
R = 100 %
FADC Bins (10 ns)

Fig. 9 a)

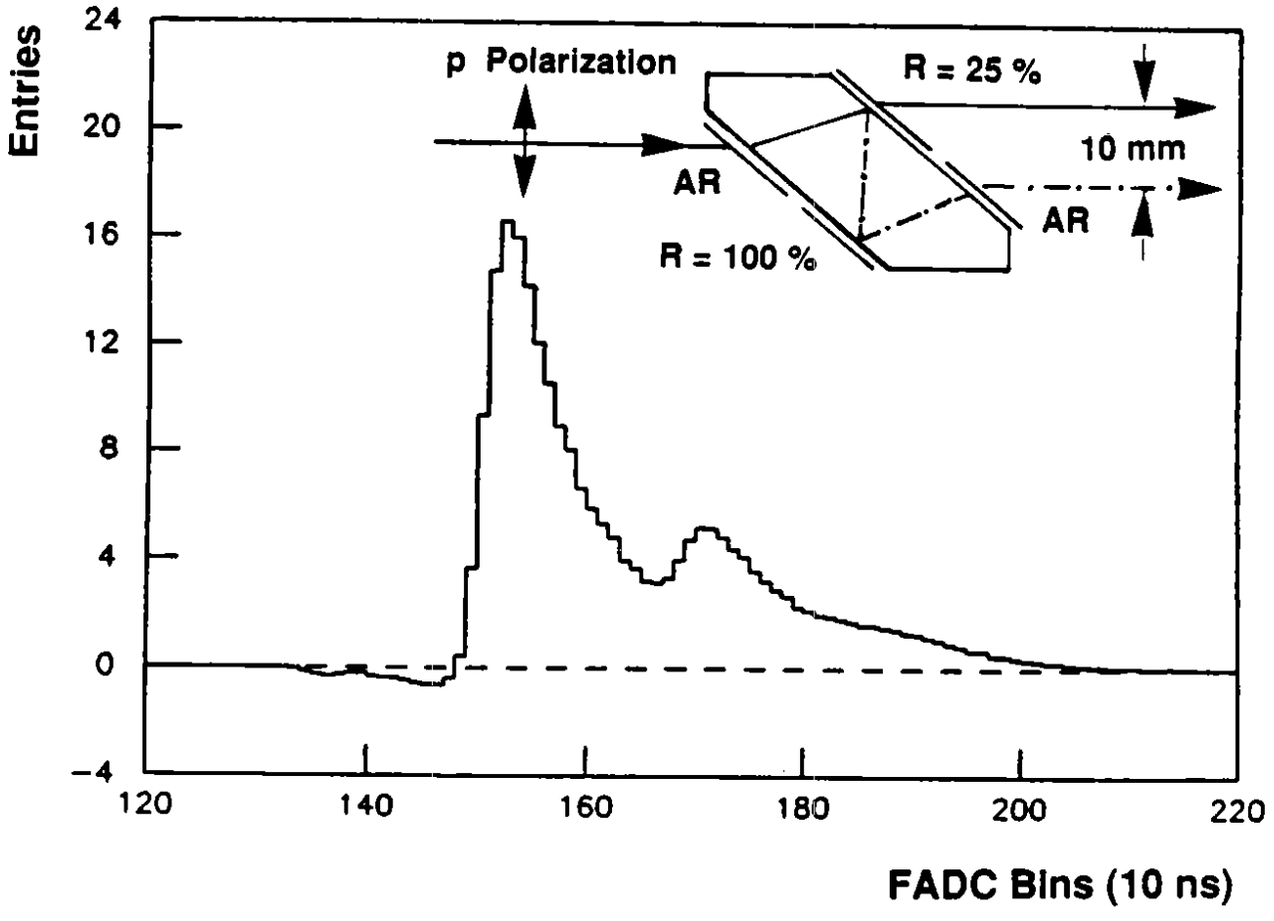
Entries
24
20
16
12
8
4
0
-4
120
140
160
180
200
220
p Polarization
R = 25 %
10 mm
AR
AR
R = 100 %
FADC Bins (10 ns)

Fig. 9 b)

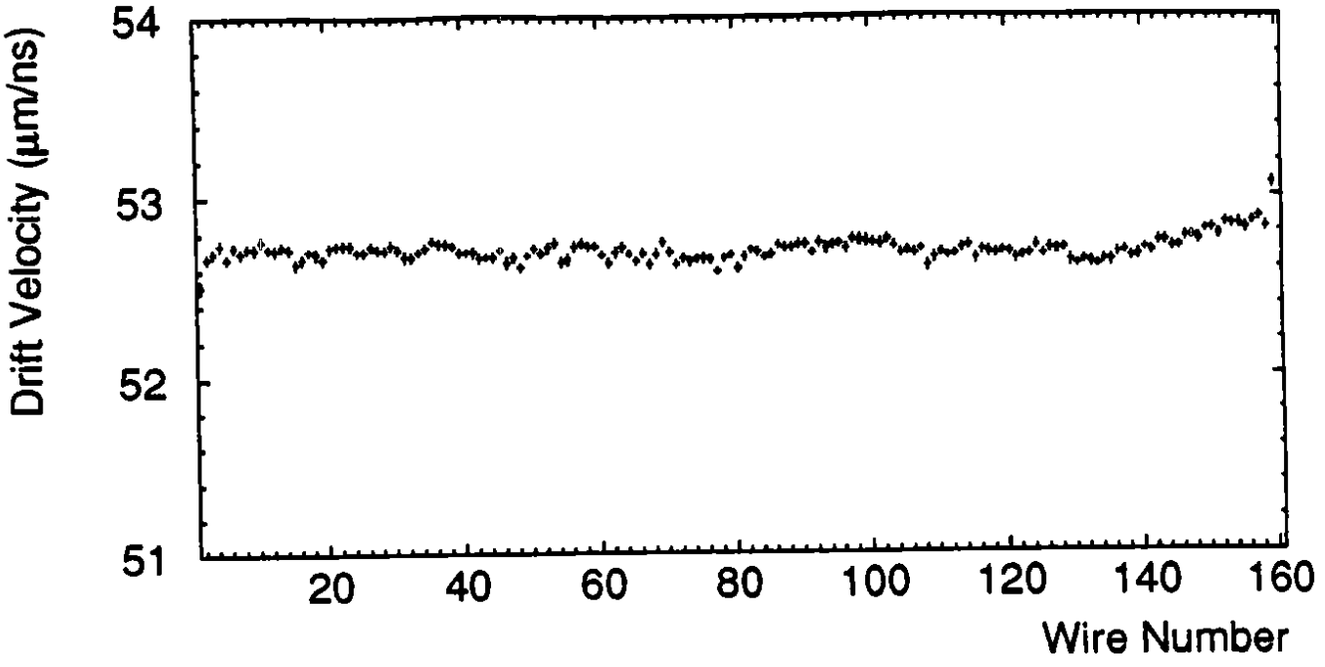

Fig. 10 a)

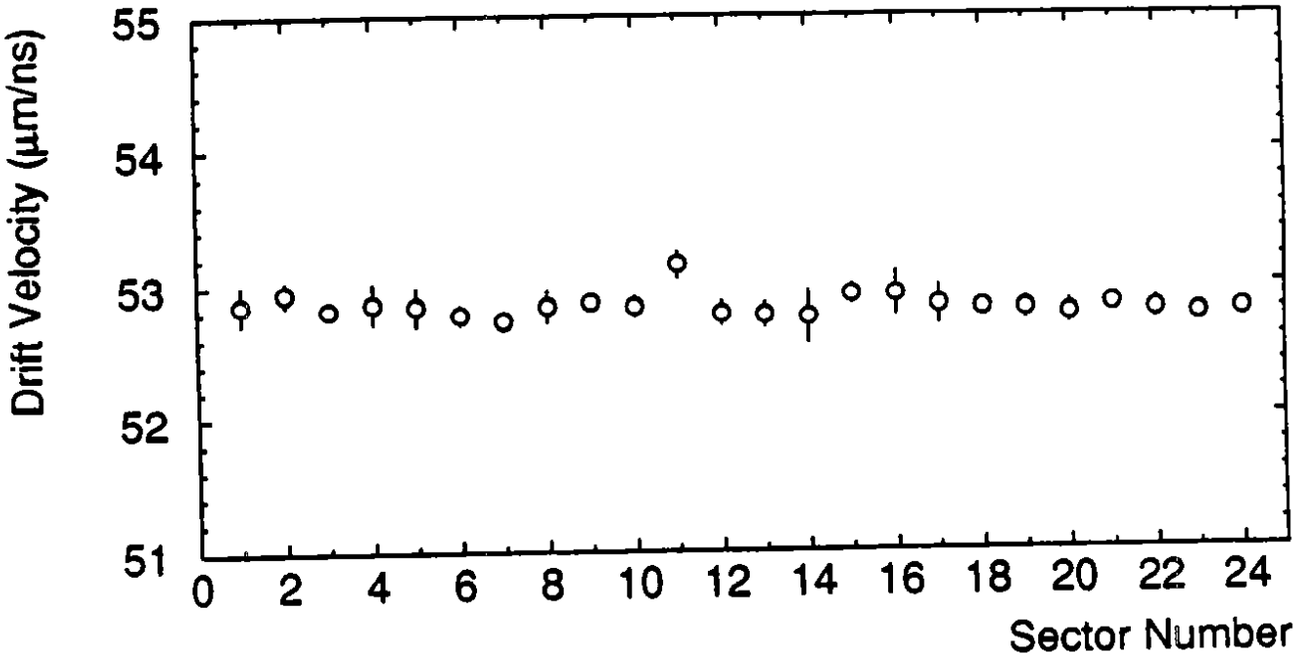

Fig. 10 b)

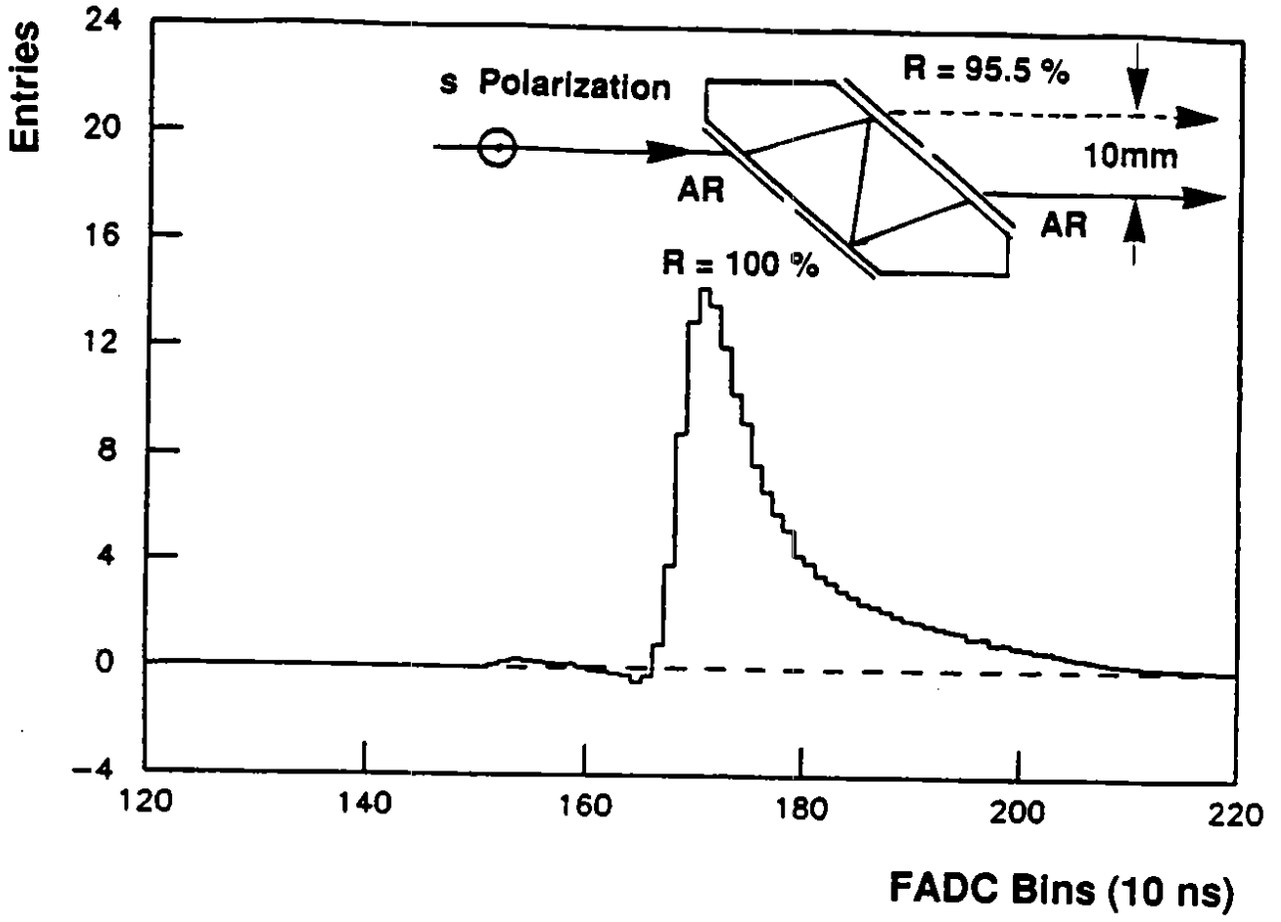
Entries
24
20
16
12
8
4
0
-4
120
140
160
180
200
220
s Polarization
R = 95.5 %
10mm
AR
AR
R = 100 %
FADC Bins (10 ns)

Fig. 9 a)

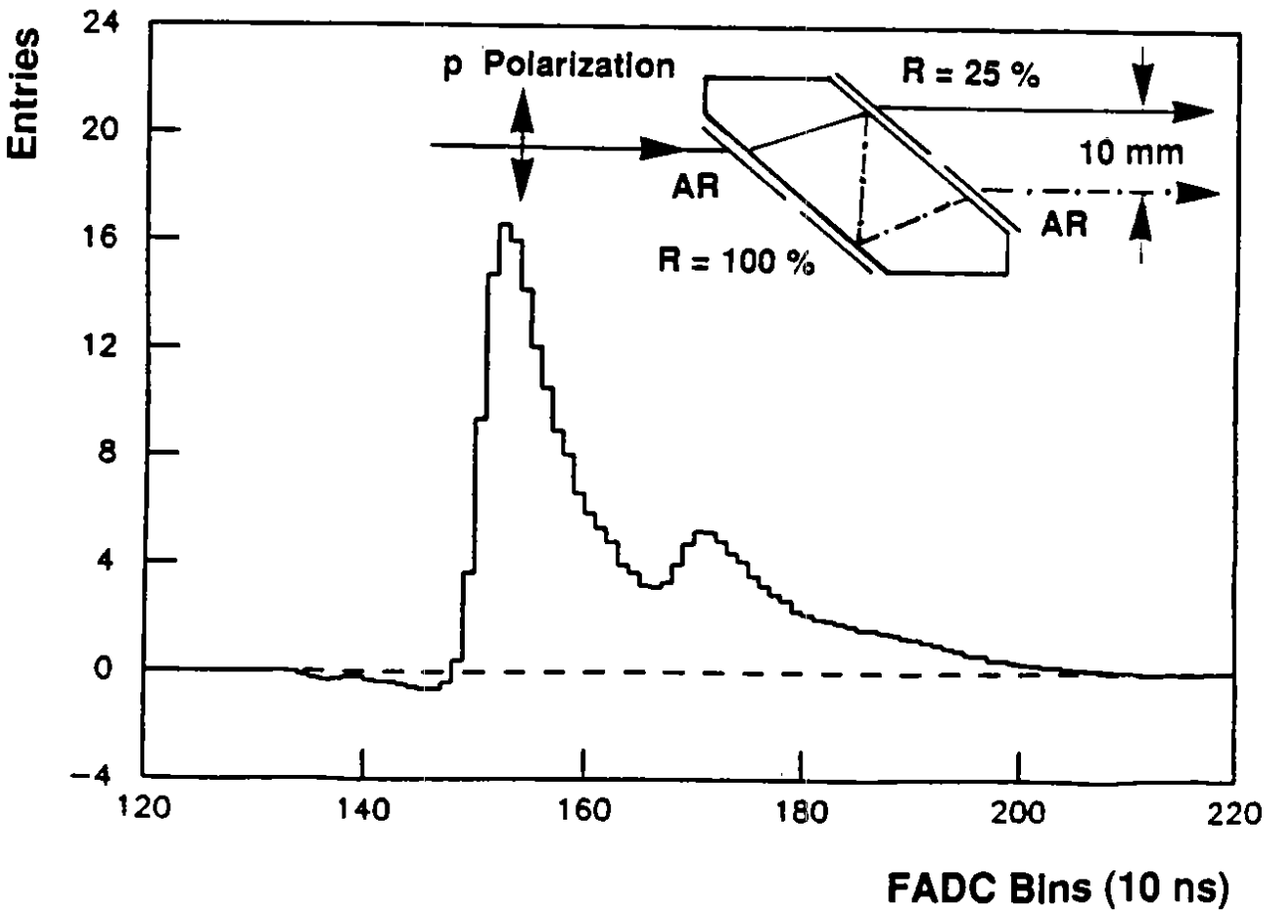
Entries
24
20
16
12
8
4
0
-4
120
140
160
180
200
220
p Polarization
R = 25 %
10 mm
AR
AR
R = 100 %
FADC Bins (10 ns)

Fig. 9 b)

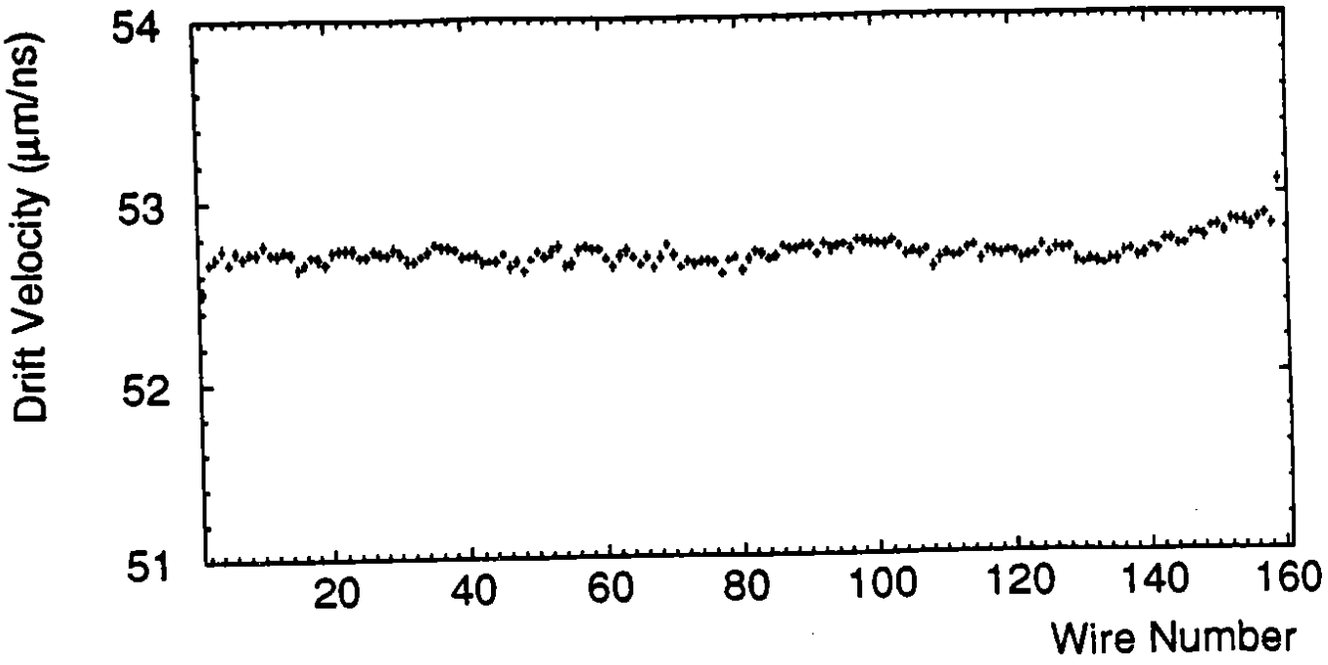

Fig. 10 a)

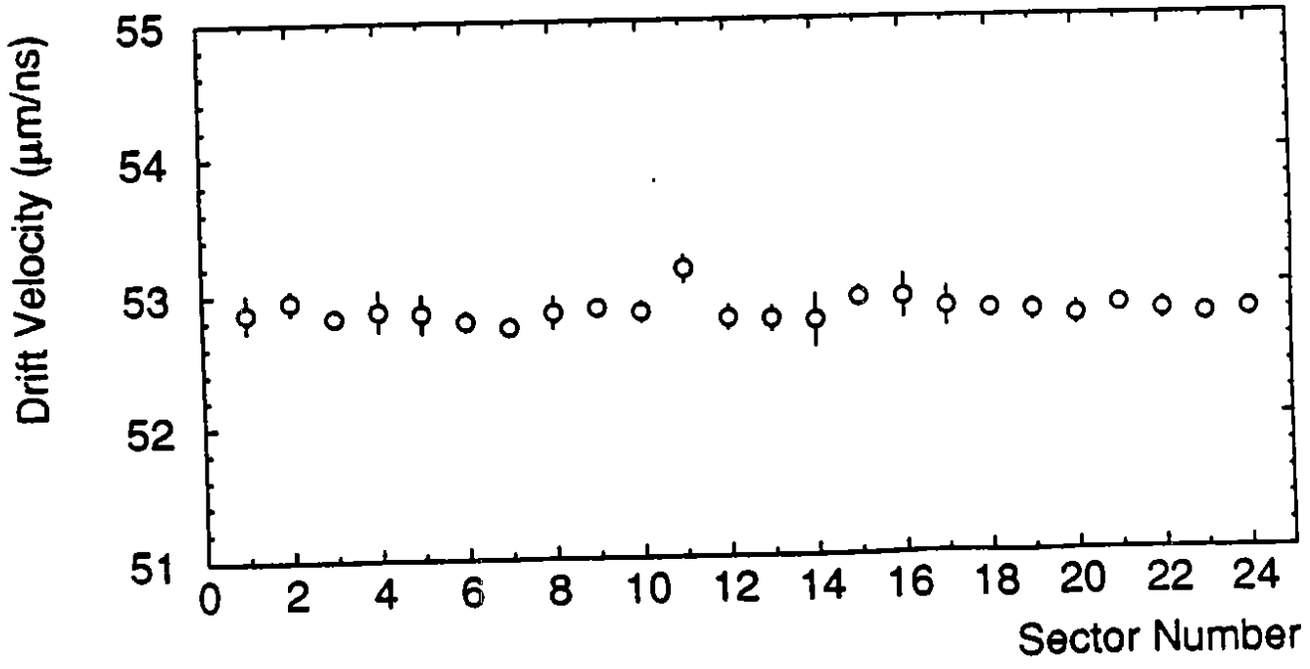

Fig. 10 b)

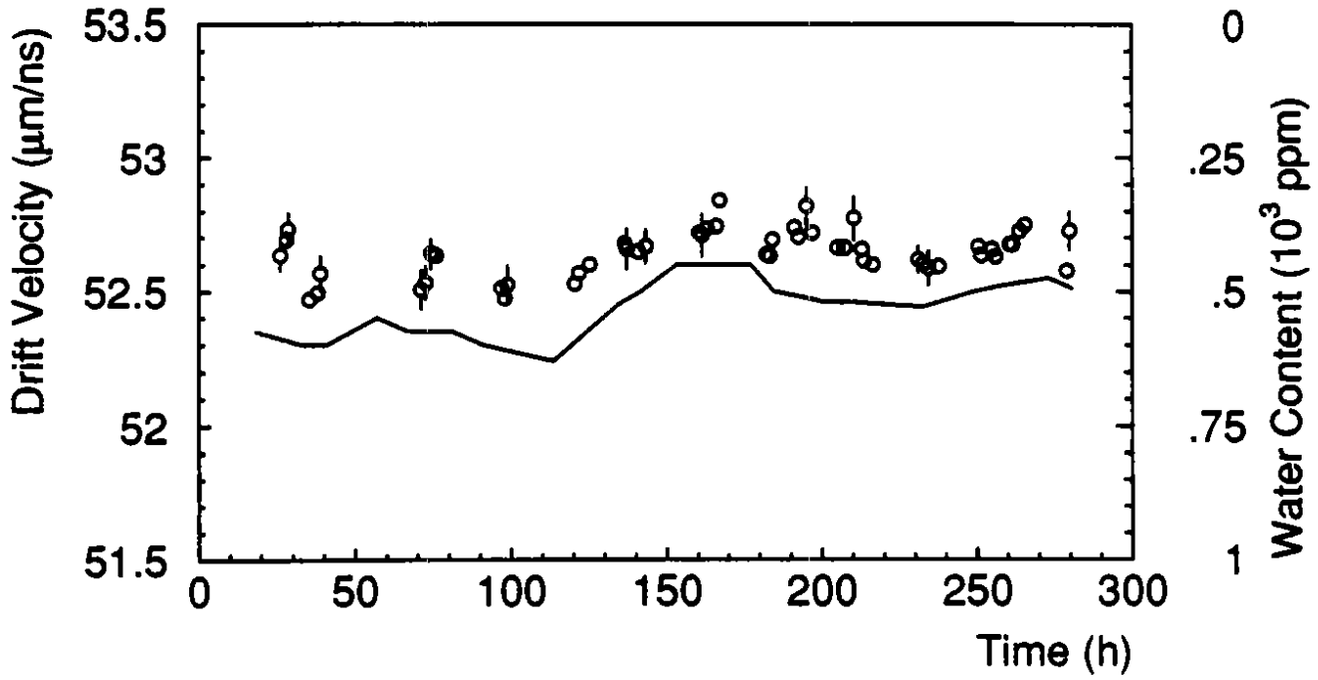
Drift Velocity (µm/ns)
53.5
53
52.5
52
51.5
0
50
100
150
200
250
300
Time (h)
0
.25
.5
.75
1
Water Content (10^3 ppm)

Fig. 11

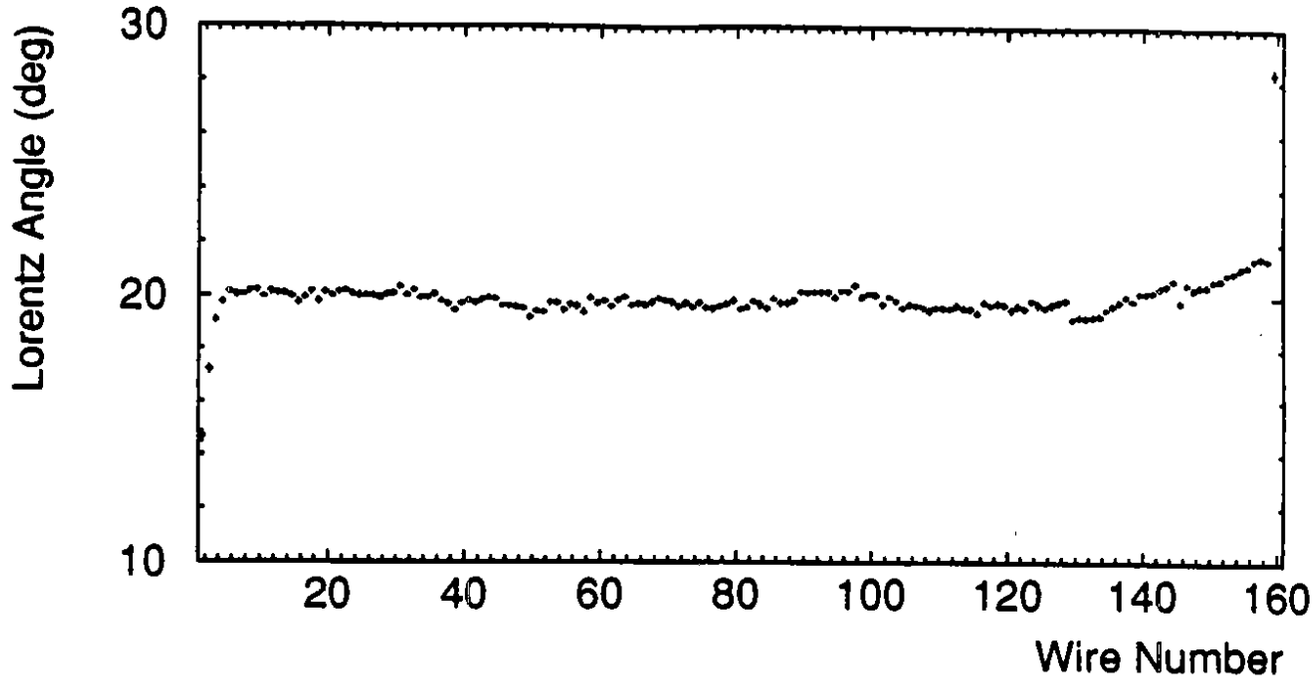

Fig. 12 a)

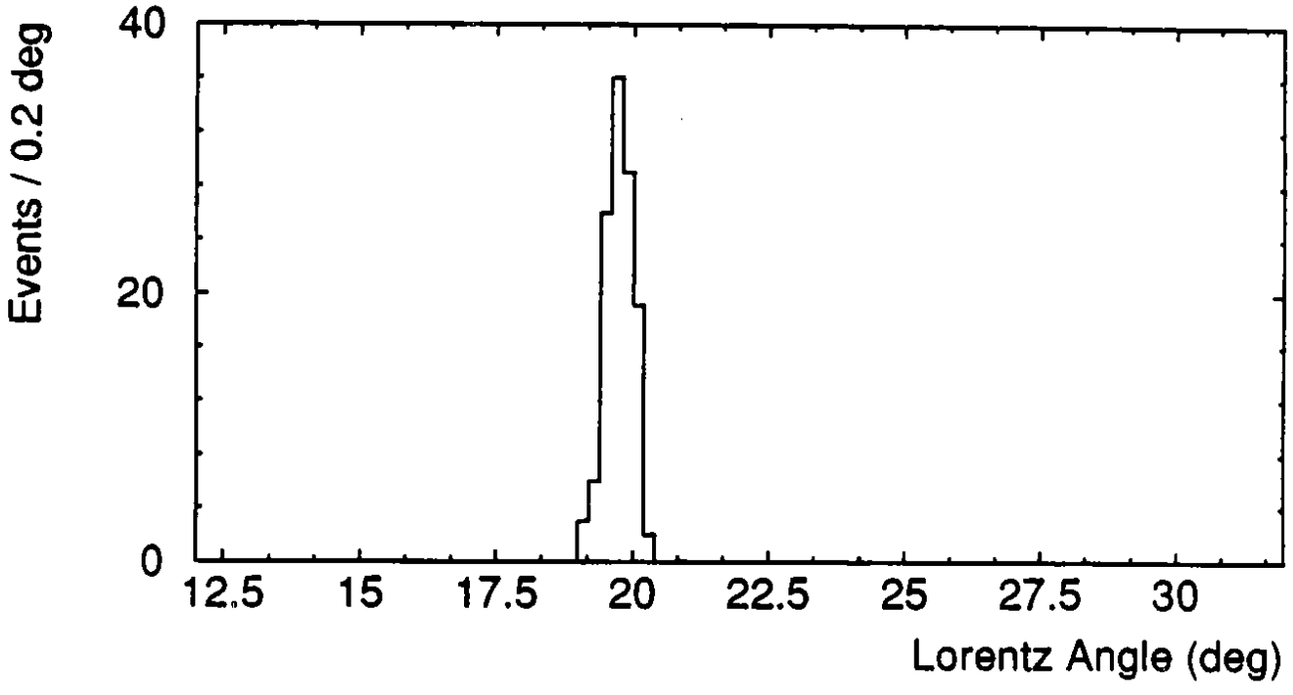

Fig. 12 b)

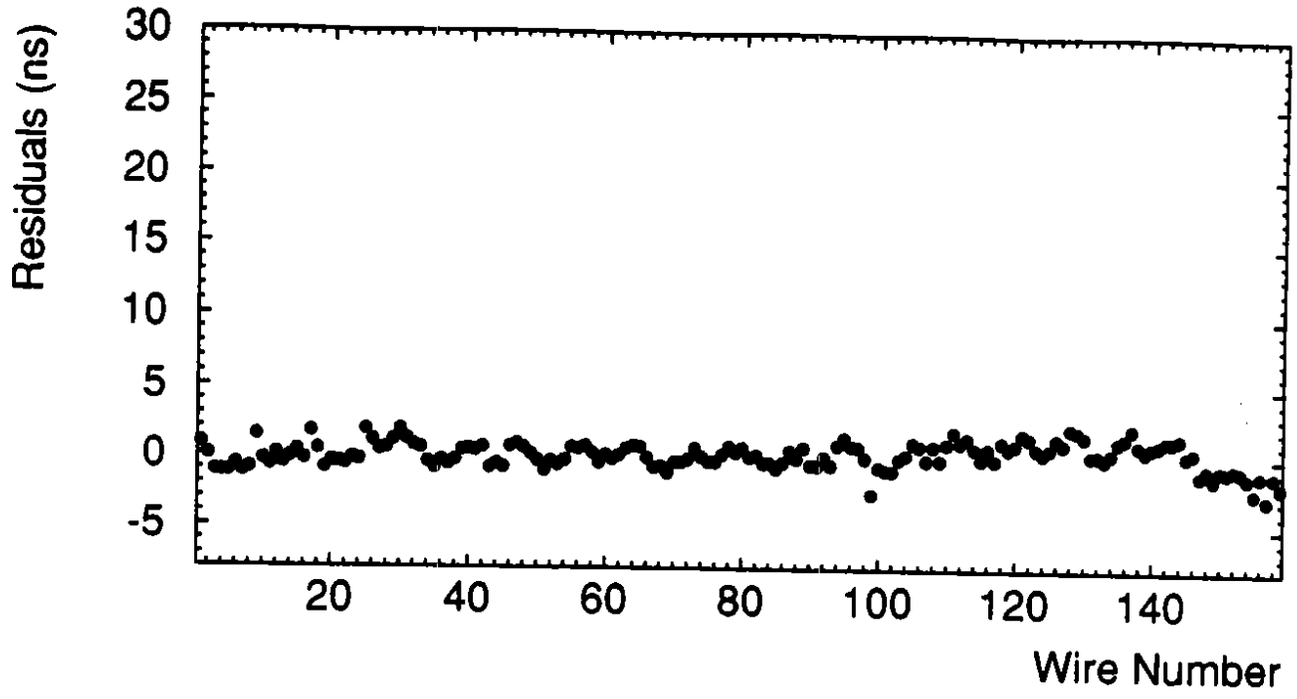

Fig. 13 a)

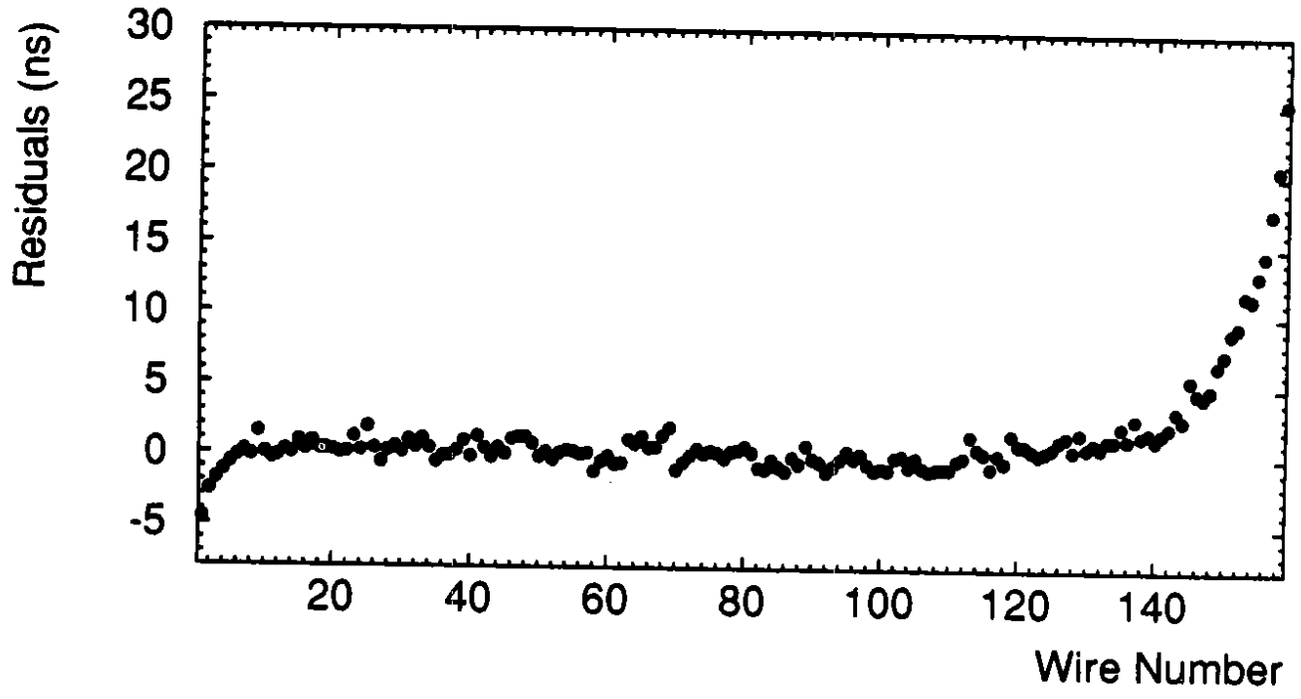

Fig. 13 b)

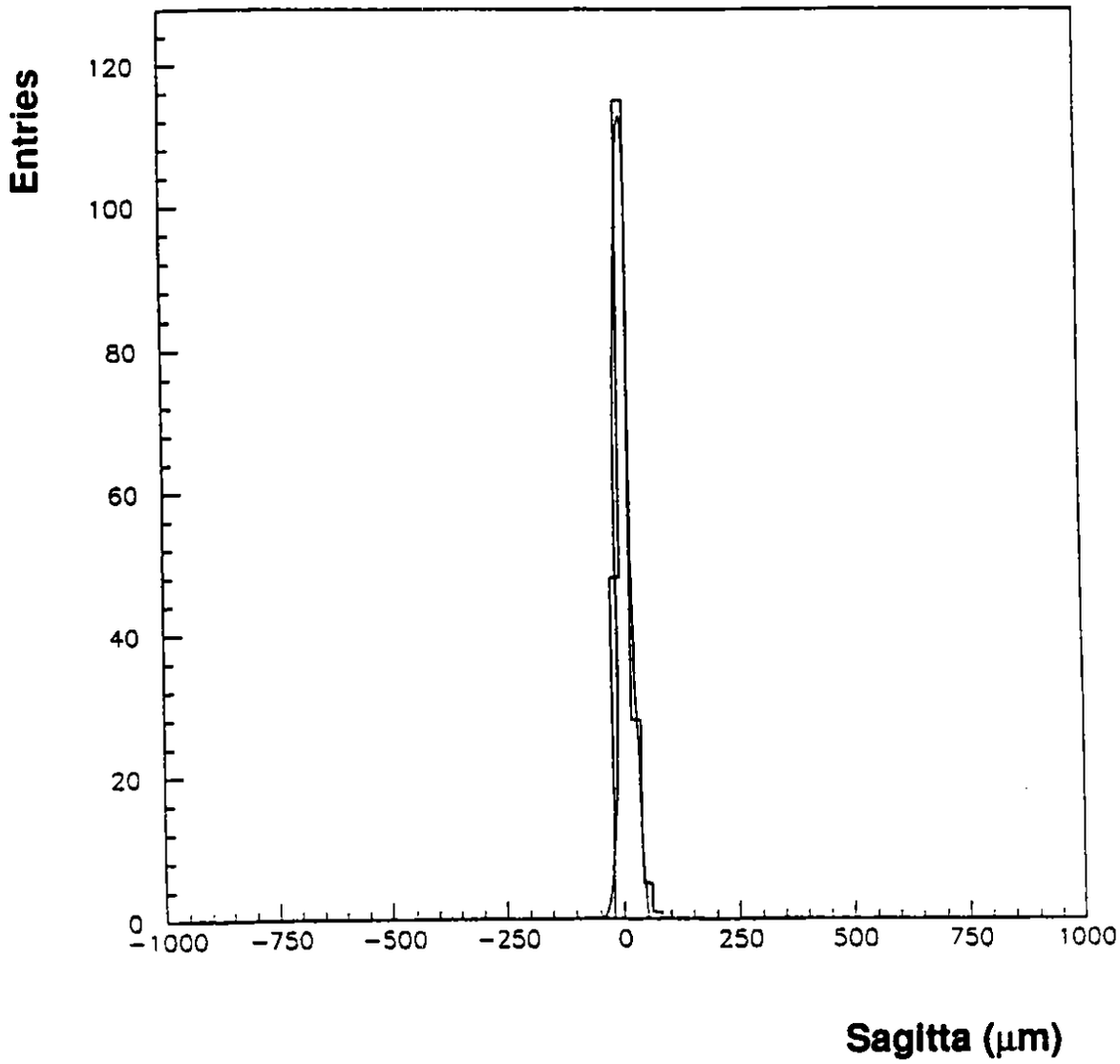
Entries
120
100
80
60
40
20
0
−1000
−750
−500
−250
0
250
500
750
1000
Sagitta (μm)

Fig. 14

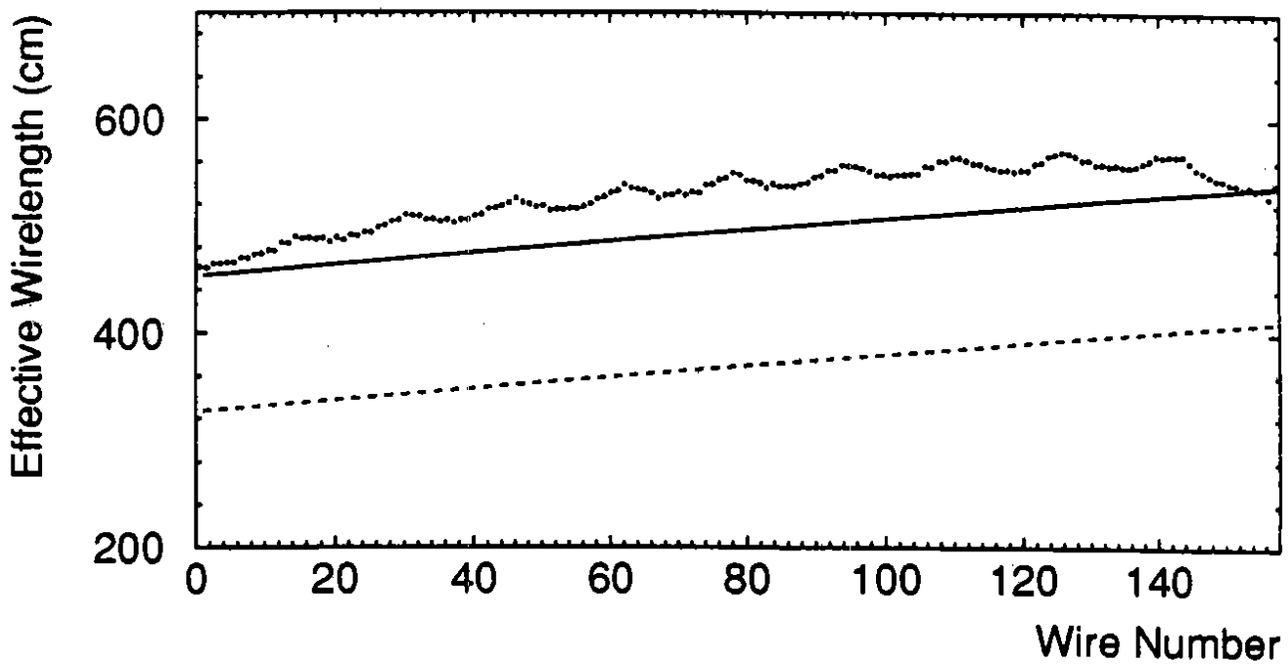
Effective Wirelength (cm)
600
400
200
0
20
40
60
80
100
120
140
Wire Number

Fig. 15

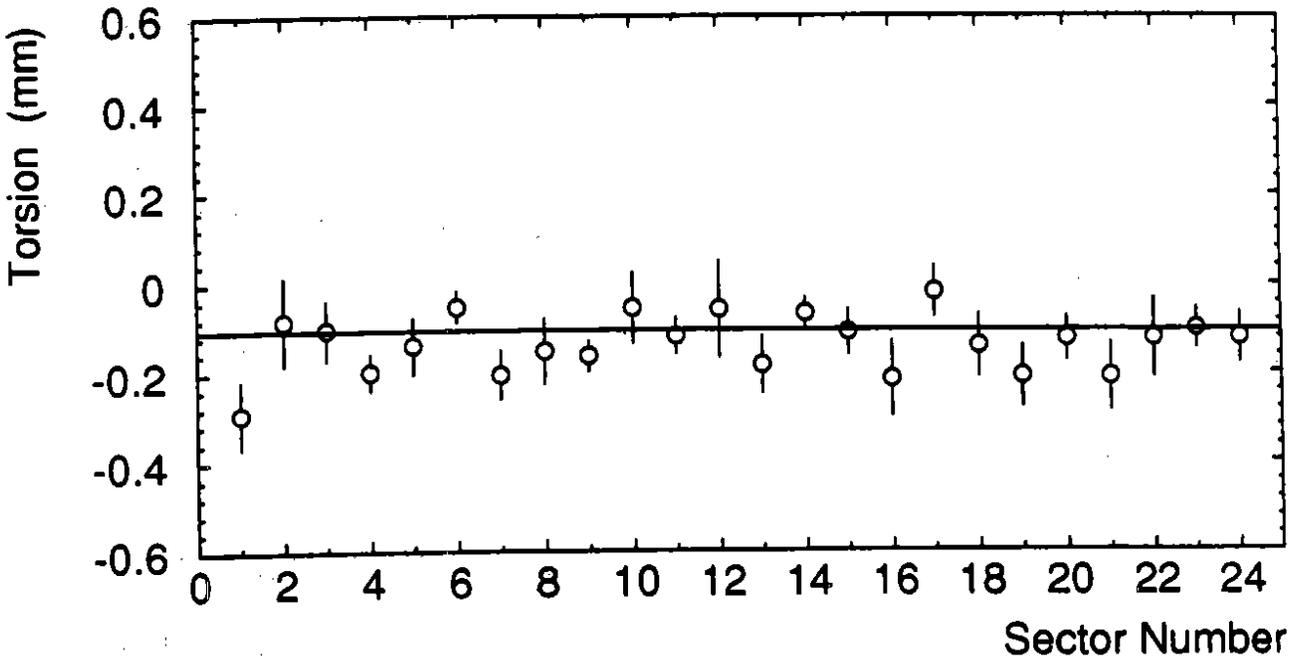
Torsion (mm)
0.6
0.4
0.2
0
-0.2
-0.4
-0.6
0
2
4
6
8
10
12
14
16
18
20
22
24
Sector Number

Fig. 16